communications biology

A Nature Portfolio journal

Article

https://doi.org/10.1038/s42003-025-08200-x

MYLIP attenuates hypoxia tolerance by inducing K27-linked polyubiquitination and subsequent proteasomal degradation of HIF-α

Jun Li[1,2,3,4], Zhi Li[1,2,3,4], Xiong Li[1,2,3,4], Ziyi Li[1,2,3,4], Yanan Song[1,2,3,4], Le Yuan[1,2,3,4], Yanyi Wang[1,2,3,4], Runkun Yan[1,2,3,4], Fuxiang Lai[1,2,3,4], Jing Wang[1,2,3,4] ✉ & Wuhan Xiao[1,2,3,4] ✉

Hypoxia tolerance is mainly controlled by the hypoxia signaling pathway and HIF-1α/2α serve as master regulators in this pathway. Here we identify MYLIP, an E3 ubiquitin ligase thought to specifically target lipoprotein receptors, as a downstream target of HIF-2α and a negative regulator of both HIF-1α and HIF-2α. MYLIP interacts with HIF-1α/2α and catalyzes K27-linked polyubiquitination at lysine 118/442 (HIF-1α) or lysine 117 (HIF-2α). This modification induces proteasomal degradation of HIF-1α, resulting in inhibition of hypoxia signaling. Furthermore, *Mylip*-deficient bluntsnout bream, zebrafish and mice are more tolerant to hypoxia. These findings reveal a role for MYLIP in regulating hypoxia signaling and identify a target for the development of fish strains with high hypoxia tolerance for the benefit of the aquaculture industry.

Aquaculture is a traditional and valuable agricultural practice in China that has now developed into a modern and high-tech industry[1]. Aquaculture in China not only provides one-third of all animal protein food, but also accounts for ~60% of the world's aquaculture production[1]. In order to reduce water pollution caused by aquaculture and to promote aquaculture products for people with increasing demand for high-quality protein, intensive and factory aquaculture will become an important trend in the future. Because fish live in water all their lives, they have a greater need for oxygen than terrestrial animals living at the same latitude, since the oxygen dissolved in water changes more frequently than that in air[2]. Cultivating fish strains or species with high oxygen tolerance is an important need for the sustainable and healthy development of the aquaculture industry. Among the seven traditional and important freshwater aquaculture species (*Ctenopharyngodon idellus*, *Hypophthalmichthys molitrix*, *Hypophthalmichthys nobilis*, *Cyprinus carpio*, *Carassius auratus*, *Megalobrama amblycephala*, and *Mylopharyngodon piceus*) in China[1], bluntsnout bream (*M. amblycephala*) is the species with the lowest hypoxia tolerance (3.0 mg/L), despite being one of the most popular aquaculture species with an annual production of ~800,000 tons. Understanding the genetic basis of hypoxia adaptation in *M. amblycephala* will help breed *M. amblycephala* strains with high hypoxia tolerance, benefiting the *M. amblycephala* aquaculture industry.

To date, it is well established that hypoxia tolerance or adaptation in animals is mainly controlled by the hypoxia signaling pathway[3]. Hypoxia-inducible factors (HIF-1α and HIF-2α) are master regulators of this pathway[4,5]. Under normoxic conditions, the HIF-α subunits (HIF1-α, HIF2-α, and HIF3-α) are hydroxylated by the prolyl hydroxylases (PHD1, PHD2, and PHD3)[5–7] and are then recognized by the von Hippel-Lindau (pVHL) tumor suppressor protein complex[4]. This complex polyubiquitylates HIF-α and targets it for proteasomal degradation. However, under hypoxic conditions, the activity of PHDs is inhibited, leading to the stabilization and accumulation of HIF-α proteins. Stabilized HIF-α proteins dimerize with HIF1β proteins, translocate to the nucleus, and induce transcription of genes involved in various biological processes[5,8]. Oxygen-dependent hydroxylation is an important mechanism for HIF-α activation[5,7]. In addition, HIF-α is also regulated by other post-translational modifications (PTMs), such as ubiquitination/deubiquitination, phosphorylation, acetylation/deacetylation, SUMOylation, methylation, S-nitrosylation, glycosylation and neddylation[9–14], which cause either increase or decrease the stability and activation of HIFα, resulting in various biological consequences[15–28].

[1]State Key Laboratory of Breeding Biotechnology and Sustainable Aquaculture, Institute of Hydrobiology, Chinese Academy of Sciences; Hubei Hongshan Laboratory, Wuhan, 430072, P. R. China. [2]Laboratory for Marine Biology and Biotechnology, Qingdao Marine Science and Technology Center, Qingdao, 266237, P. R. China. [3]University of Chinese Academy of Sciences, Beijing, 100049, P. R. China. [4]The Innovation of Seed Design, Chinese Academy of Sciences, Wuhan, 430072, P. R. China. ✉e-mail: wangjing@ihb.ac.cn; w-xiao@ihb.ac.cn

MYLIP, also known as the inducible degrader of the LDL receptor (IDOL), has been identified as a RING E3 ubiquitin ligase that promotes the ubiquitylation and subsequent lysosomal degradation of the LDL receptor (LDLR), thereby limiting the uptake of lipoprotein-derived cholesterol into cells and thus playing an important role in the regulation of lipoprotein metabolism in vivo[29,30]. To date, MYLIP also induces ubiquitination-dependent degradation of the very LDL receptor (VLDLR) and apolipoprotein E receptor 2 (APOER2) in addition to the LDLR, suggesting a role for MYLIP in systematic energy balance and proper neuronal migration and positioning[31–34]. It is poorly known whether MYLIP is unique in having such narrow and specific targets or has a broader spectrum of ubiquitination targets like most other E3s.

In this study, we found that MYLIP is induced by hypoxia and serves as a downstream target of HIF-2α, which promotes proteasomal degradation of both HIF-1α and HIF-2α. Mechanistic studies suggest that MYLIP targets HIFα at a lysine residue (K118/442 in HIF1α; K117 in HIF-2α) to catalyze K27-linked polyubiquitination. Furthermore, disruption of *Mylip* in bluntsnout bream, zebrafish, and mice promotes hypoxia tolerance in these animals, suggesting that we have identified an important target for gene editing to produce hypoxia-tolerant strains of bluntsnout bream in the aquaculture industry.

Results

Disruption of *mylipb* in fish promotes hypoxia tolerance

We have previously shown that disruption of the repressors of the hypoxia signaling pathway promotes hypoxia tolerance in zebrafish[35–37], although this is not always the case[38], and we are interested in identifying the hypoxia-induced E3 ubiquitin ligases in the bluntsnout bream (*M. amblycephala*), which may target the key factors of the hypoxia signaling pathway for proteasomal degradation and serve as good candidates for engineering hypoxia-tolerant strains of *M. amblycephala* by gene editing. After transcriptome analysis, we found that *mylipb* but not *mylipa* is the highest E3 ubiquitin ligase induced by hypoxia in *M. amblycephala*, which was further confirmed by quantitative RT-PCR assays (Supplementary Fig. 1a, b). It was also found that *mylipb* is expressed at higher levels in the brain and intestine of *M. amblycephala* (Supplementary Fig. 1c) and is evolutionarily conserved in its amino acid sequence and protein structure (Supplementary Fig. 1d–g).

To quickly know whether *mylipb* affects hypoxia tolerance, we first knocked out *mylipb* in *M. amblycephala* using CRISPR/Cas9 and tested hypoxia tolerance in *M. amblycephala* with *mylipb* disruption (Supplementary Fig. 2a–e). Since it takes 2 to 3 years for *M. amblycephala* to reach sexual maturity, we first attempted to test hypoxia tolerance in $mylipb^{+/-}$ *M. amblycephala*. No abnormal phenotypes were observed in $Mylipb^{+/-}$ *M. amblycephala*. Compared to wild-type *M. amblycephala*, $mylipb^{+/-}$ *M. amblycephala* were more tolerant to hypoxia (Supplementary Fig. 2f and 2g; Supplementary Video 1). The classical hypoxia-inducible genes, including *phd3*, *glut1*, *pkd2*, and *vegfa*[2], were significantly increased in $mylipb^{+/-}$ *M. amblycephala*, suggesting that the hypoxia signaling pathway is affected by *mylipb* (Supplementary Fig. 2h–k).

To further validate the role of *mylipb* in hypoxia tolerance, we wanted to know what happens in fish with a complete loss of *mylipb*. We therefore turned to the zebrafish model. Indeed, zebrafish *mylipb* was also induced under hypoxia and highly expressed in zebrafish brain (Supplementary Fig. 3a–c). We took advantage of the *mylipb* knockout zebrafish line[39]. $mylipb^{-/-}$ zebrafish were indistinguishable from their wild-type siblings in development, growth, maturation, and reproduction. Compared to wild-type zebrafish larvae ($mylipb^{+/+}$), $mylipb^{-/-}$ larvae had more erythrocytes under hypoxia as shown by both O-dianisidine staining and Tg(*gata1*:eGFP)-labeling (Fig. 1a–d). Consistently, *epoa* was more highly expressed in $mylipb^{-/-}$ larvae compared to $mylipb^{+/+}$ larvae under hypoxia (Fig. 1e). Hypoxia treatment caused more deaths in $mylipb^{+/+}$ than $mylipb^{-/-}$ zebrafish larvae and adults (Fig. 1f–i; Supplementary Video 2). As expected, the classical hypoxia-inducible genes, including *phd3*, vegfa, *glut1*, *pdk1*, and *ldha*, were dramatically increased in $mylipb^{-/-}$ larvae and adult brain (Fig. 1j, k; Supplementary Fig. 4a–f).

Taken together, these data suggest that disruption of the hypoxia-induced E3 ubiquitin ligase, *mylipb*, promotes hypoxia tolerance in the bluntsnout bream and zebrafish, and affects the hypoxia signaling pathway.

MYLIP attenuates hypoxia signaling

To investigate the underlying mechanism of *mylipb* in hypoxia tolerance, we turned to the mammalian system, where more antibodies, cell lines, and research tools are available than in fish.

In mammals, there is only one *MYLIP* gene instead of two. First, we confirmed that mammalian MYLIP was also induced by hypoxia in H1299 and A549 cells, and that hypoxia induced *MYLIP* expression in H1299 cells to a lesser extent compared to that in A549 cells (Fig. 2a). Therefore, we next used H1299 cells to overexpress *MYLIP* but used A549 cells to knock out *MYLIP*.

Notably, hypoxia induced *MYLIP* expression at levels comparable to typical hypoxia-responsive genes, *PDK1, GLUT1*, and *VEGF*, in A549 cells (Fig. 2b). We further confirmed that the addition of a specific PHD hydroxylase inhibitor, FG4592, also induced *MYLIP* expression to a similar extent as *PDK1, GLUT1*, and *VEGF* (Fig. 2c). The hypoxia-inducible expression of *MYLIP* was validated by Western blot analysis (Fig. 1d). We then investigated whether *MYLIP* is indeed a direct hypoxia-inducible factor-activated gene. Two putative hypoxia response elements (HRE) exist in the promoter of MYLIP (5'-GCGTG-3') (Fig. 2e). Overexpression of *HIF-2α*, but not of *HIF-1α* activated the luciferase reporter activity of the *MYLIP* promoter, suggesting that MYLIP might be a specific downstream target of HIF-2α, but not of HIF-1α (Fig. 2f). When the second HRE, but not the first HRE in the promoter of MYLIP was mutated (pGL3-MYLIP-mut2), both hypoxia treatment and overexpression of HIF-2α did not activate the mutated promoter reporter activity in H1299 cell (Fig. 2g). The specific HIF-1α inhibitor, PAX478, did not suppress *MYLIP* expression, but the specific HIF-2α inhibitor, Belzutifan, was able to suppress *MYLIP* expression (Fig. 2h). The specific inhibitory roles of PAX478 and Belzufan was confirmed by examining the expression of *LDHA* (a HIF-1α downstream target) and *CITED2* (a HIF-2α downstream target), respectively (Fig. 2h). Chromatin immunoprecipitation (ChIP) assay showed that HIF-2α, but not HIF-1α bound to the MYLIP promoter (Fig. 2i). The *LDHA* promoter was used as a control for HIF-1α binding (Fig. 2i). Therefore, MYLIP may be a direct HIF-2α-transactivated downstream gene.

With prolonged exposure of A549 cells to hypoxia, HIF-1α and HIF-2α protein levels were stabilized from 12 to 24 h and decreased after 36 h of hypoxia treatment (Supplementary Fig. 5a). Consistently, MYLIP protein levels were also increased from 12 h, remained stable until 24 h, and decreased after 36 h of hypoxia treatment (Supplementary Fig. 5a). The mRNA and protein levels of MTLIP were consistent in response to hypoxia treatment (Supplementary Fig. 5b). The expression of the downstream target of HIF-1α, *LDHA*, was steadily induced from 12 h to 24 h, and then decreased from 36 h of hypoxia treatment (Supplementary Fig. 5c). Interestingly, the expression of the specific downstream target of HIF-2α, *CITED2*, was induced to the highest level at 12, but decreased from 24 h of hypoxia treatment, when HIF-2α and MYLIP protein levels were still maintained at higher levels (Supplementary Fig. 5d). It appeared that MYLIP could interfere with the transcriptional activity of HIF-2α, leading to a decrease in *CITED2* expression. To further test whether MYLIP is a specific target of HIF-2α, we used Belzutifan to block HIF-2α transcriptional activity and found that *LDHA* was still induced by hypoxia, but *MYLIP* and *CITED2* were not upregulated after hypoxia treatment (Supplementary Fig. 5e–h).

We then investigated whether mammalian *MYLIP* affects hypoxia signaling. Overexpression of *MYLIP* in H1299 cells dramatically reduced the expression of hypoxia-inducible genes under hypoxia, including *PDK1, GLUT1, EPO* and *VEGF* (Fig. 3a, b; Supplementary Fig. 6a). In contrast, knockout of *MYLIP* in A549 cells increased the expression of hypoxia-inducible genes under hypoxia (Fig. 3c, d; Supplementary Fig. 5b). In addition, overexpression of *MYLIP* suppressed the activity of HRE− and typical hypoxia-inducible gene promoter-driven luciferase reporters

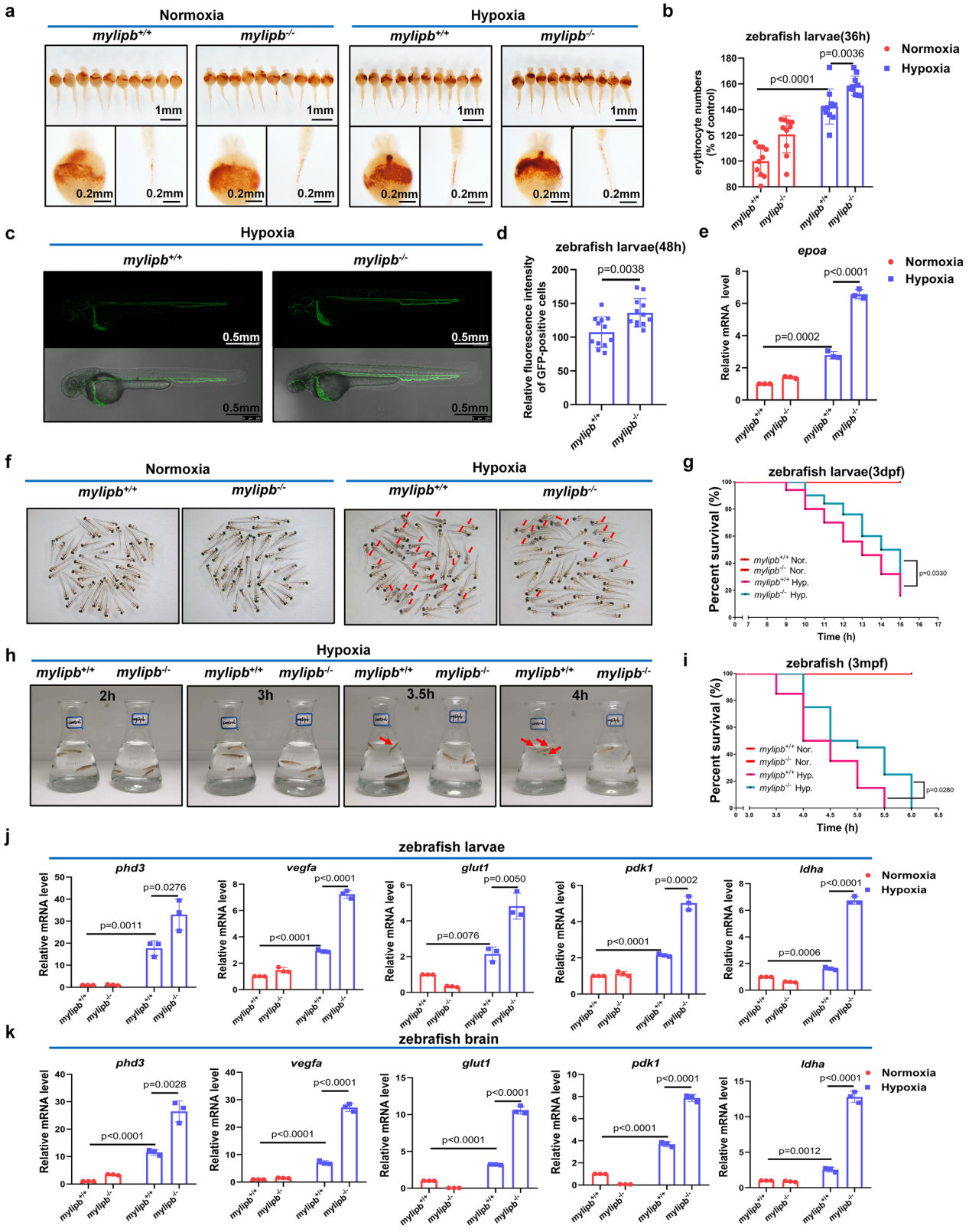

(Supplementary Fig. 6c–f). Consistently, the addition of FG4592 to block the activity of PHDs enhanced the expression of hypoxia-inducible genes, including *PDK1, GLUT1, VEGF,* and *EPO* (Fig. 3e).

Taken together, these data suggest that mammalian MYLIP may serve as a direct downstream target of HIF-2α to attenuate hypoxia signaling.

MYLIP interacts with HIF-1α to induce HIF-1α degradation independent of the EGLN-pVHL pathway

Since *HIF-1α* is a master regulator of hypoxia signaling, we first investigated whether *MYLIP* affects its activity. Overexpression of *MYLIP* induces the degradation of co-expressed HA-HIF-1α in a dose-dependent manner (Supplementary Fig. 7a). In addition, overexpression of *MYLIP* significantly

Fig. 1 | Disruption of *mylipb* in zebrafish promotes hypoxia tolerance. **a** O-dianisidine staining of functional hemoglobin in the erythrocytes of *mylipb*$^{+/+}$ and *mylipb*$^{-/-}$ zebrafish larvae (36 hpf) under normoxia (21% O_2) or hypoxia (10% O_2) for 10 h. **b** The number of erythrocytes increased in *mylipb*$^{-/-}$ compared to *mylipb*$^{+/+}$ zebrafish larvae (36 hpf) under hypoxia (10% O_2) for 10 h ($n = 10$ each group). **c** Fluorescence images of Tg(*gata1*:eGFP)/*mylipb*$^{+/+}$ and Tg(*gata1*:eGFP)/*mylipb*$^{-/-}$ showed that *mylipb*$^{-/-}$ zebrafish larvae (48 hpf) have more *gata1*-positive erythrocytes under hypoxia (10% O_2) for 10 h. **d** Quantitation of *gata1*-positive erythrocytes in Tg(*gata1*:eGFP)/*mylipb*$^{+/+}$ and Tg(*gata1*:eGFP)/*mylipb*$^{-/-}$ zebrafish larvae (48 hpf) under hypoxia (10% O_2) for 10 h ($n = 12$ per group). **e** qPCR analysis of *epoa* mRNA in *mylipb*$^{+/+}$ or *mylipb*$^{-/-}$ zebrafish larvae under hypoxia (2% O_2) for 6 h. **f** Images of *mylipb*$^{+/+}$ and *mylipb*$^{-/-}$ zebrafish larvae (3 dpf, $n = 50$ per group) under normoxia (21% O_2) or hypoxia (2% O_2) for 12 h. The dead larvae (marked by red arrows) showed a lack of movement, a lack of blood circulation, and physical degeneration. **g** Survival curve of *mylipb*$^{+/+}$ and *mylipb*$^{-/-}$ zebrafish larvae (3 dpf, $n = 50$ each group) under hypoxia (2% O_2) for 15 h. Statistical analysis was performed using the Gehan-Breslow-Wilcoxon test. **h** Images of *mylipb*$^{+/+}$ and *mylipb*$^{-/-}$ adult zebrafish (3 mpf, $n = 3$ per group) after 2, 3, 3.5, and 4 h under hypoxia (5% O_2). Red arrows indicate dying zebrafish. **i** Survival curve of *mylipb*$^{+/+}$ and *mylipb*$^{-/-}$ adult zebrafish (3 mpf, $n = 20$ each group) under hypoxia (5% O_2) for 6 h. Statistical analysis was performed using the Gehan-Breslow-Wilcoxon test. **j** qPCR analysis of *phd3, vegfa, glut1, pdk1, ldha* mRNA in *mylipb*$^{+/+}$ or *mylipb*$^{-/-}$ zebrafish larvae under hypoxia (2% O_2) for 6 h. **k** qPCR analysis of *phd3, vegfa, glut1, pdk1, ldha* mRNA in the brain of *mylipb*$^{+/+}$ or *mylipb* $^{-/-}$ adult zebrafish (3 mpf) under hypoxia (5% O_2) for 3 h. Data in (**b**, **d**) are presented as mean ± S.D., two-tailed Student's t test. Data in (**e**, **j**, **k**) are presented as mean ± S.D., two-tailed Student's *t* test; $n = 3$ biologically independent experiments.

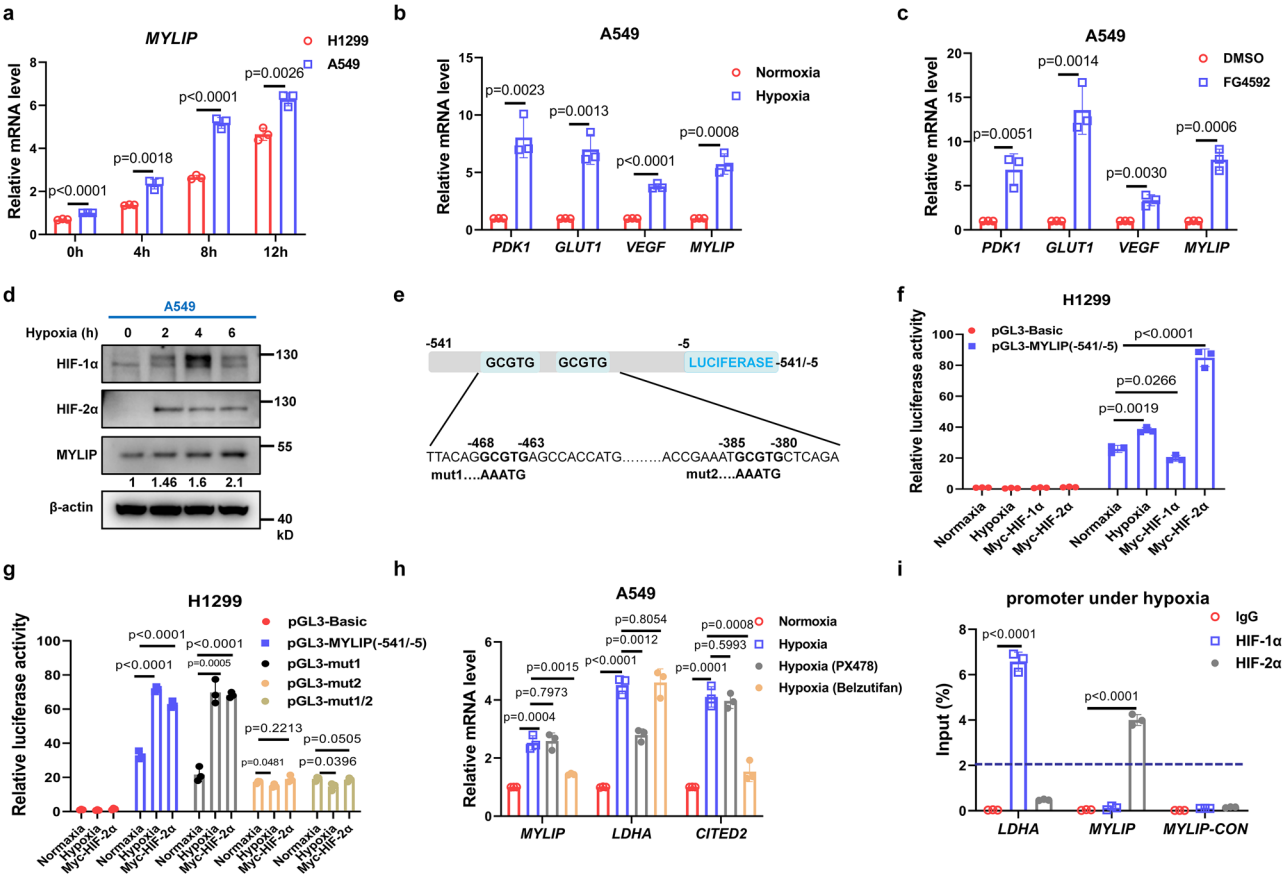

Fig. 2 | Hypoxia induces *MYLIP* expression. **a** qPCR analysis of *MYLIP* mRNA in H1299 cells and A549 cells under normoxia (21% O_2) or hypoxia (1% O_2) for 4, 8, 12 h. **b** qPCR analysis of *PDK1*, *GLUT1*, *VEGF*, and *MYLIP* mRNA in A549 cells under normoxia (21% O_2) or hypoxia (1% O_2) for 18 h. **c** qPCR analysis of *PDK1*, *GLUT1*, *VEGF*, and *MYLIP* mRNA in A549 cells treated with FG4592 (100 μM) or DMSO as a control for 8 h. **d** Western blot analysis of the indicated proteins in A549 cells under normoxia (21% O_2) or hypoxia (1% O_2) for 2, 4, 6 h. **e** Schematic of the potential hypoxia responsive element (HRE) (GCGTG) localized at the *MYLIP* promoter (−541 to −5). **f** The luciferase activity of *MYLIP* promoters induced by hypoxia (1% O_2 for 16 h) or overexpression of Myc-HIF-1α or Myc-HIF-2α in H1299 cells. **g** The luciferase activities of different *MYLIP* promoters induced by hypoxia (1% O_2 for 16 h) or overexpression of Myc-HIF-2α in H1299 cells. **h** qPCR analysis of *MYLIP*, *LDHA* and *CITED2* mRNA in A549 cells treated with PX478 (100 μM) or Belzutifan (100 μM) under hypoxia (1% O_2) for 18 h. **i** A549 cells under hypoxia (1% O_2) for 24 h. ChIP assays were performed with IgG, anti-HIF-1α, or anti-HIF-2α antibodies. Data in (**a**–**c**, **f**–**i**) are presented as mean ± S.D., two-tailed Student's *t* test; $n = 3$ biologically independent experiments. Data in (**d**) are representative of three independent experiments.

suppresses the hypoxia-induced activity of the HRE-driven luciferase reporter (Supplementary Fig. 7b).

We then found that overexpressed *MYLIP* interacted with endogenous HIF-1α, and endogenous MYLIP interacted with endogenous HIF-1α in VHL-deficient H1299 cells (*VHL*$^{-/-}$) (Fig. 4a, b). Bacterially expressed His-MYLIP also interacted with bacterially expressed GST-HIF-1α by GST pull-down assays, suggesting that MYLIP directly interacts with HIF-1α (Fig. 4c). Domain mapping revealed that the RING domain of MYLIP is required for binding to HIF-1α (Supplementary Fig. 8a, b). Consistent with the above overexpression assays (Supplementary Fig. 7a), HIF-1α protein levels are higher in *MYLIP*$^{-/-}$ A549 cells than in *MYLIP*$^{+/+}$ A549 cells under hypoxia (Fig. 4d). In *VHL*$^{-/-}$ H1299 cells, the addition of FG4592 eliminated HIF-1α hydroxylation, but overexpression of *MYLIP* still reduced HIF-1α protein levels, suggesting that MYLIP-induced HIF-1α degradation is independent of the PHD-pVHL pathway (Fig. 4e). We further confirmed that the proline and asparagine hydroxylation mediated by the proline hydroxylases (PHD1, PHD2 and PHD3) or the asparagine hydroxylase (FIH) is not required for MYLIP-induced HIF-1α degradation (Fig. 4f), in contrast to the mechanism

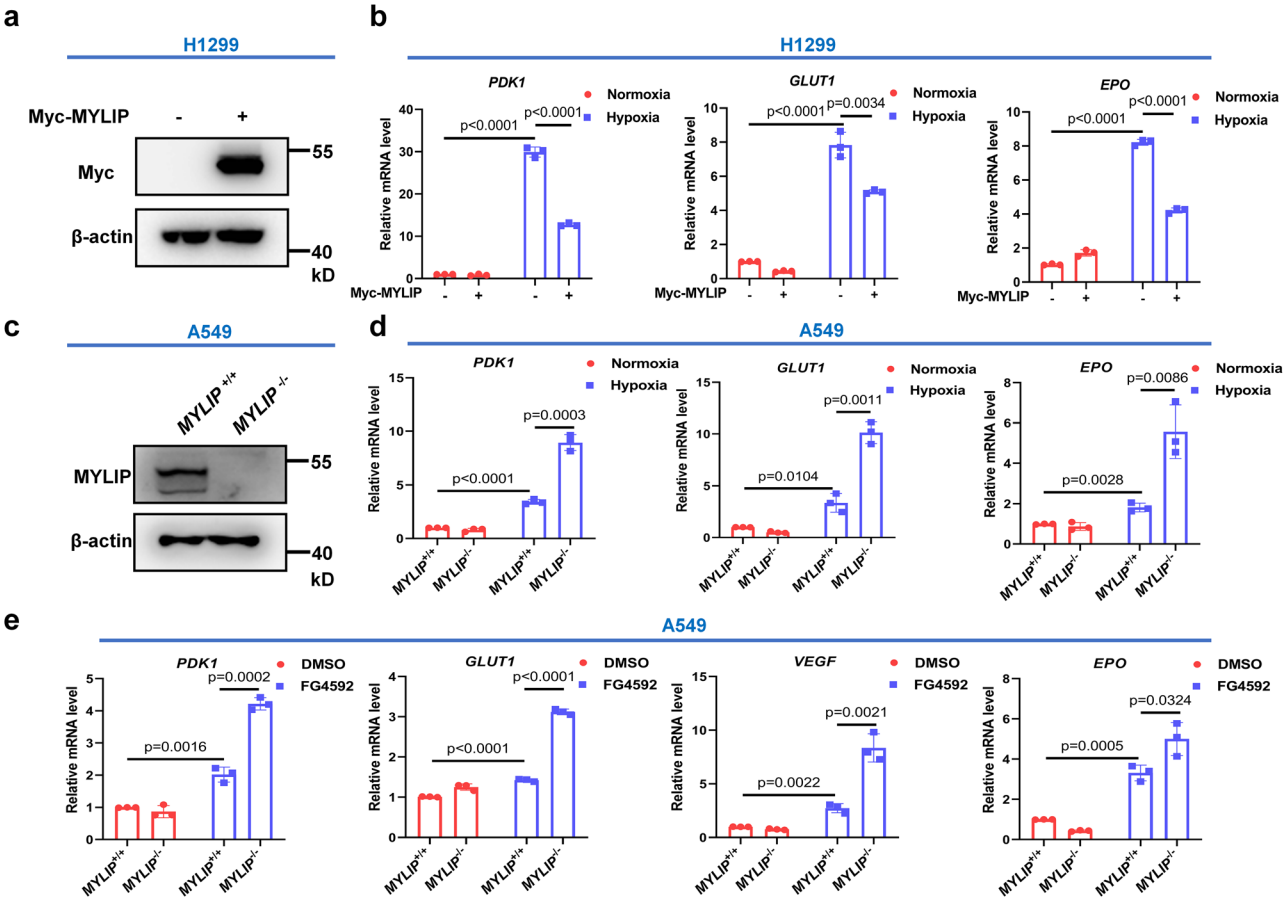

Fig. 3 | *MYLIP* attenuates hypoxia signaling. a Western blot analysis of the indicated proteins in H1299 cells transfected with or without Myc-*MYLIP*. **b** qPCR analysis of *PDK1*, *GLUT1*, and *EPO* mRNA in H1299 cells under normoxia (21% O_2) or hypoxia (1% O_2) for 18 h. **c** Western blot analysis of the indicated proteins in wild-type or *MYLIP*-deficient A549 cells ($MYLIP^{+/+}$ or $MYLIP^{-/-}$). **d** qPCR analysis of *PDK1*, *GLUT1*, and *EPO* mRNA in $MYLIP^{+/+}$ *or* $MYLIP^{-/-}$ A549 cells under normoxia (21% O_2) or hypoxia (1% O_2) for 18 h. **e** qPCR analysis of *PDK1*, *GLUT1*, *VEGF* and *EPO* mRNA in $MYLIP^{+/+}$ or $MYLIP^{-/-}$ A549 cells treated with FG4592 (100 μM) or DMSO as a control for 8 h. Data in (**a**, **c**) are representative of three independent experiments. Data in (**b**, **d**, **e**) are presented as mean ± S.D., two-tailed Student's *t* test; *n* = 3 biologically independent experiments.

induced by the VHL E3 ubiquitin ligase complex, a classical pathway for mediating HIF-1α degradation under normoxia[40]. The protein level of HIF-1α was still found to be higher in $MYLIP^{-/-}$ cells than in $MYLIP^{+/+}$ cells treated with FG4592 (Fig. 4g). Furthermore, when cycloheximide (CHX) was used to block new protein synthesis, HIF-1α remained stable longer in $MYLIP^{-/-}$ A549 cells than in $MYLIP^{+/+}$ A549 cells under hypoxia (Fig. 4h, i).

Furthermore, we confirmed that the stabilized HIF-1α in $MYLIP^{-/-}$ A549 cells was mainly distributed in the nucleus instead of the cytosol, suggesting that the stabilization of HIF-1α by disruption of MYLIP can indeed enhance the transcriptional activity of HIF-1α (Fig. 4j, k).

Taken together, these data suggest that MYLIP induces HIF-1α degradation independently of the PHD-pVHL pathway.

MYLIP targets HIF-1α at lysine 118 and 442 to catalyze K27-linked polyubiquitination and induce subsequent proteasomal degradation of HIF-1α

We then investigated what type of degradation of HIF-1α is mediated by MYLIP using various inhibitors, including MG-132, NH_4Cl, 3-MA, chloroquine, and Bafilomycin A1 (BafA1). Addition of MG-132 efficiently blocked HIF-1α degradation induced by overexpression of *MYLIP*, but other inhibitors did not, suggesting that *MYLIP* may induce proteasomal degradation of HIF-1α (Fig. 5a; Supplementary Fig. 9a). To rule out the influence of other proteins on drug treatment effects, we repeated the inhibitor treatment without the MYLIP overexpression, no difference was found between different inhibitor treatments (Supplementary Fig. 9b). Because *MYLIP* is a well-defined E3 ubiquitin ligase[29], we generated its enzyme-deficient mutant, MYLIP (C387S)[29,33], and found that the mutant (MYLIP-C/S) did not induce HIF-1α degradation like wild-type MYLIP (Fig. 5b, c). Consistently, the mutant was unable to catalyze poly-ubiquitination of endogenous HIF-1α (Fig. 5d). In vitro ubiquitination assay showed that MYLIP can directly catalyze HIF-1α ubiquitination (Fig. 5e). Furthermore, overexpression of *MYLIP-C/S* did not suppress hypoxia signaling at the level of wild-type *MYLIP*, suggesting that the enzymatic activity of MYLIP is required for its suppressive function on the hypoxia signaling (Supplementary Fig. 10a–c). We found that MYLIP specifically catalyzed the K27-linked polyubiquitination of exogenous and endogenous HIF-1α (Fig. 5f–h).

To determine which lysine (s) is (are) targeted by MYLIP for poly-ubiquitination, we generated a series of mutants, in which all lysine residues of HIF-1α were mutated to arginine residues, respectively, and examined their stability when *MYLIP* was co-expressed (Supplementary Fig. 11a, b). Two mutants, K118R and K442R, were apparently not degraded by *MYLIP* overexpression (Supplementary Fig. 11b). The site, K118 site is evolutionarily conserved from zebrafish to human, but K442 is not conserved in zebrafish hif-1αa (Supplementary Fig. 12). Protein structure prediction showed that K118 is localized inside the HIF-1α protein, and K442 is localized outside of the HIF-1α protein (Fig. 5i).

When K118 and K442 were simultaneously mutated to arginine, K118/442 R, this double mutant was not degraded at all by MYLIP (Fig. 5j).

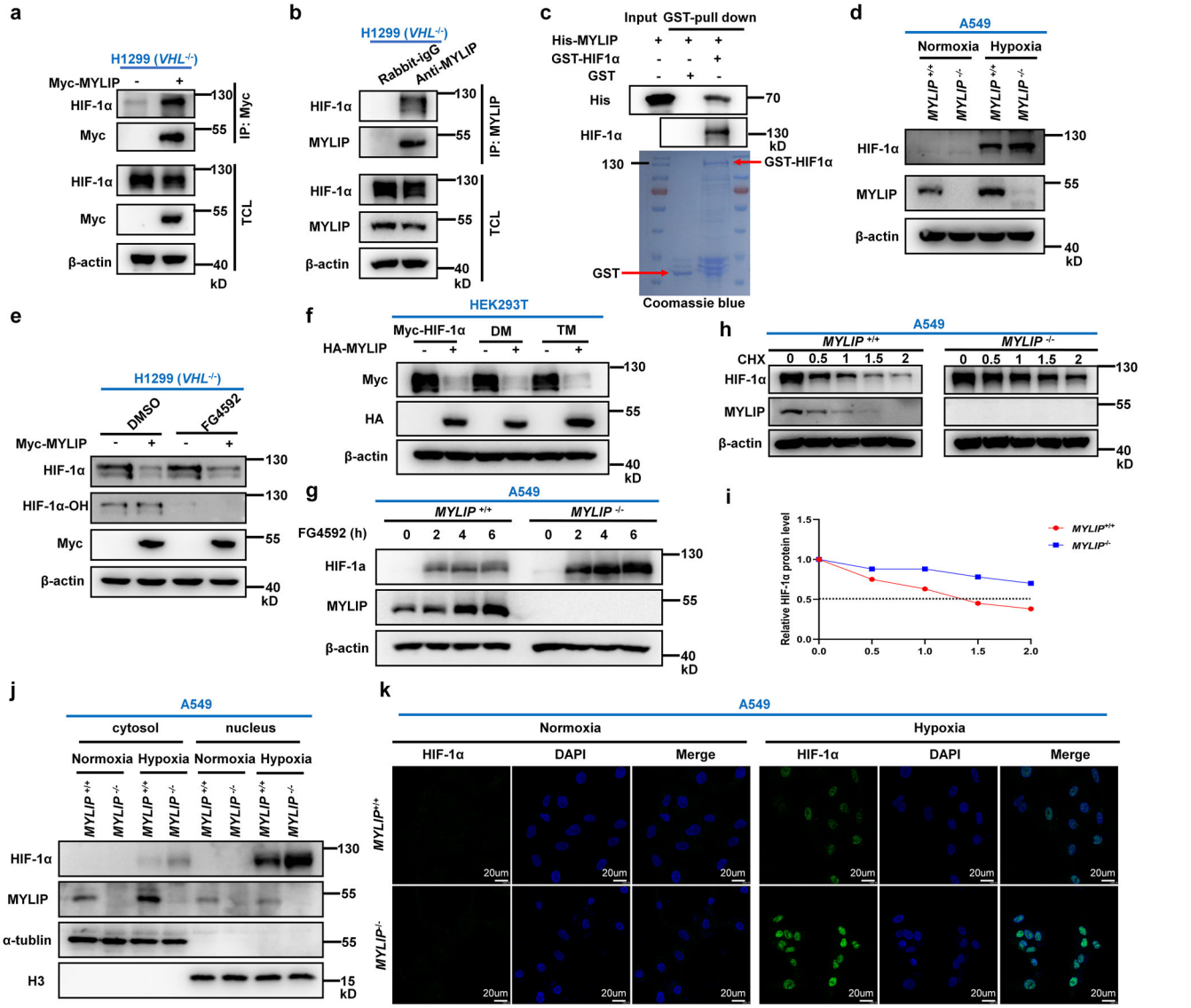

Fig. 4 | MYLIP interacts with HIF-1α to induce HIF-1α degradation. **a** Immunoprecipitation of Myc-*MYLIP* with endogenous HIF-1α. H1299 (*VHL*$^{-/-}$) cells were transfected with the indicated plasmids and cultured under normoxia (21% O_2) for 24 h. Anti-Myc antibody-conjugated agarose beads were used for immunoprecipitation, and the interaction was detected by immunoblotting with the indicated antibodies. **b** Endogenous interaction of MYLIP with HIF-1α in H1299 (*VHL*$^{-/-}$) cells. Anti-MYLIP antibody was used for immunoprecipitation, and normal rabbit IgG was used as a control. **c** GST pull-down assay for the interaction of GST-tagged HIF-1α with His-MYLIP. GST-HIF-1α and His-MYLIP were expressed in *Escherichia coli* (BL21). The association of GST-HIF-1α with His-MYLIP was detected by immunoblotting with anti-His antibody. GST and GST-HIF-1α proteins were stained with Coomassie Blue. **d** Western blot analysis of the indicated proteins in *MYLIP*$^{+/+}$ or *MYLIP*$^{-/-}$ A549 cells under normoxia (21% O_2) or hypoxia (1% O_2) for 4 h. **e** Western blot analysis of the indicated proteins in H1299 (*VHL* $^{-/-}$) cells transfected with the empty vector control (Myc empty) or Myc-*MYLIP* and treated with FG4592 (100 μM) or DMSO as a control for 4 h. **f** Western blot analysis of the indicated proteins in HEK293T cells transfected with Myc-*HIF-1α*, Myc-*HIF-1α*-DM, or Myc-*HIF-1α*-TM together with the HA-empty or HA-*MYLIP*. **g** Western blot analysis of endogenous HIF-1α in *MYLIP*$^{+/+}$ or *MYLIP* $^{-/-}$ A549 cells in the presence of FG4592 (100 μM) for 0, 2, 4, 6 h. **h** Western blot analysis of endogenous HIF1α in *MYLIP*$^{+/+}$ or *MYLIP*$^{-/-}$ A549 cells in the presence of cycloheximide (CHX, 50 μg/ml) for 0, 0.5, 1, 1.5, 2 h under hypoxia (1% O_2). **i** The relative intensities of HIF-1α in (**g**) were determined by normalizing the intensities of HIF-1α to the intensities of β-actin. **j** Western blot analysis of HIF-1α in cytosol and nuclear fractions in *MYLIP*$^{+/+}$ or *MYLIP*$^{-/-}$ A549 cells. *MYLIP*$^{+/+}$ or *MYLIP*$^{-/-}$ A549 cells were cultured under normoxia (21% O_2) or hypoxia (1% O_2) for 4 h. **k** Confocal microscopy image of endogenous HIF-1α in *MYLIP*$^{+/+}$ or *MYLIP*$^{-/-}$ A549 cells under normoxia (21% O_2) or hypoxia (1% O_2) for 4 h. Scale bar = 20 μm. Data in (**a**, **b**, **j**, **d**–**h**) are representative of three independent experiments.

Consistently, MYLIP-catalyzed K27-linked polyubiquitination was significantly reduced in the single mutants K118R and K442R compared to that on wild-type HIF-1α, but was completely eliminated in the double mutant K118/442R (Fig. 5k).

Taken together, these data suggest that MYLIP targets HIF-1α at lysine 118 and 442 to catalyze K27-linked polyubiquitination and induce subsequent proteasomal degradation of HIF-1α, leading to inhibition of hypoxia signaling.

MYLIP targets HIF-2α at lysine 117 to catalyze K27-linked polyubiquitination, resulting in inhibition of HIF-2α activity

We then investigated whether MYLIP also affects HIF-2α in a similar way to HIF-1α. We found that MYLIP binds to HIF-2α and also noticed that K118 is evolutionarily conserved in HIF-2α (K117) (Supplementary Fig. 13a, d). Similar to HIF-1α, HIF-2α was higher in *MYLIP*$^{-/-}$ A549 cells than in *MYLIP*$^{+/+}$ A549 cells under hypoxia (Supplementary Fig. 13b). Consistently, *MYLIP* overexpression induced HIF-2α degradation in H1299

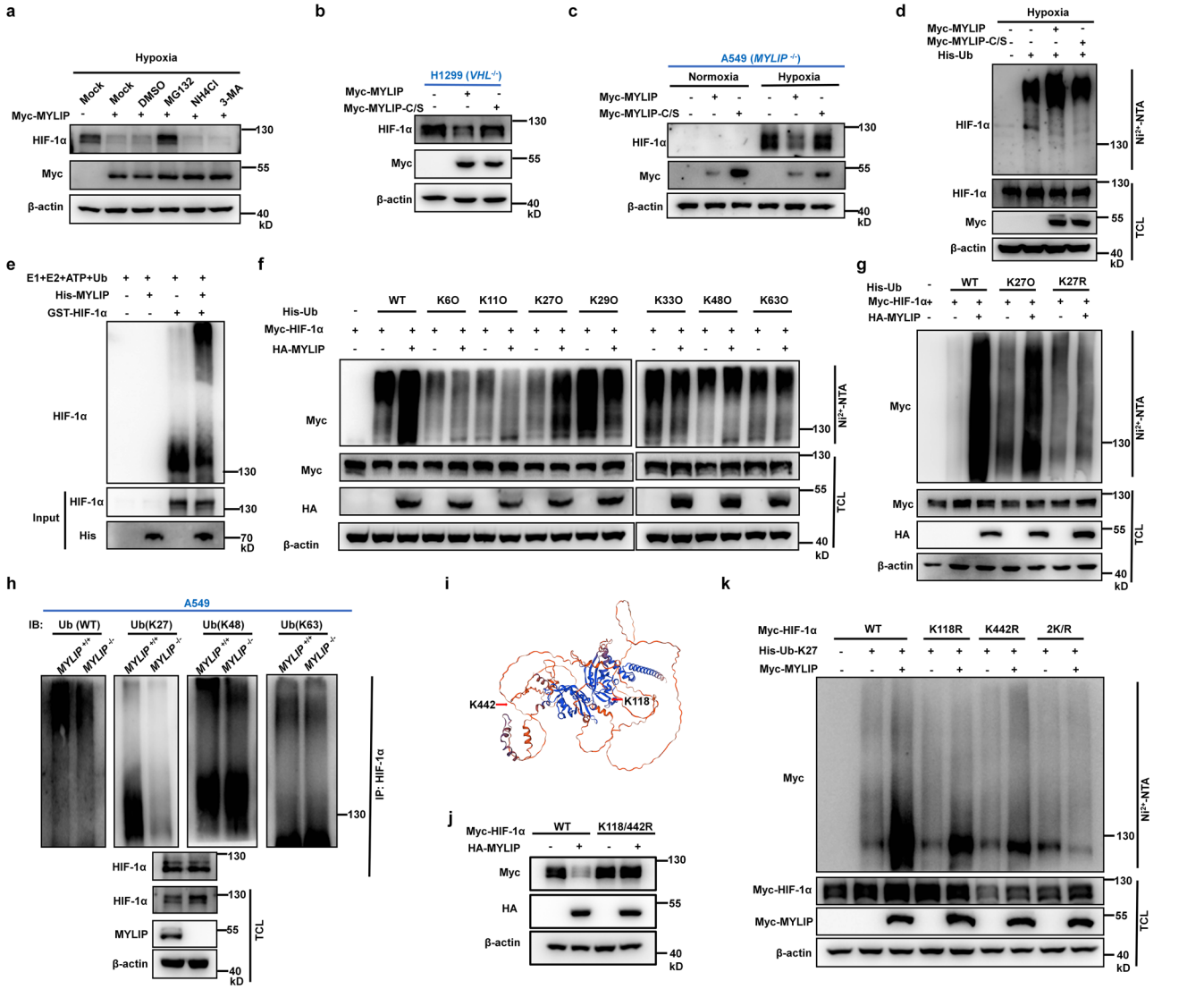

Fig. 5 | MYLIP targets HIF-1α at Lys118 and Lys442 to catalyze K27-linked polyubiquitination. a Western blot analysis of the indicated proteins in HEK293T cells transfected with Myc-*MYLIP* in the presence of DMSO (control), MG-132 (20 μM), NH_4Cl (5 mM), or 3-MA (1 mM) under hypoxia (1% O2) for 6 hours. **b** Western blot analysis of the indicated proteins in H1299 (*VHL*$^{-/-}$) cells transfected with Myc-*MYLIP* or its enzyme-deficient mutant (C387S) (Myc-*MYLIP*-C/S). **c** Western blot analysis of the indicated proteins in A549 (*MYLIP*$^{-/-}$) cells transfected with Myc-*MYLIP* or Myc-*MYLIP*-C/S under normoxia (21% O_2) or hypoxia (1% O_2) for 4 h. **d** Endogenous HIF-1α ubiquitination in HEK293T cells transfected with Myc empty, Myc-*MYLIP*, or Myc-*MYLIP*-C/S, in the presence of His-Ub-WT and treated with MG-132 (20 μM) for 6 hours under hypoxia (1% O_2). **e** In vitro ubiquitination assay. The purified GST-HIF-1α proteins were used in an in vitro ubiquitination reaction in the presence of E1, E2 (UbcH5A, UbcH5B, UbcH5C), Ub, and His-MYLIP. **f** HIF-1α ubiquitination in HEK293T cells transfected with Myc-HIF-1α and HA-*MYLIP*, in the presence of His-tagged wild-type ubiquitin (WT), or the mutant ubiquitins, including K6-only (K6O), K11-only(K11O), K27-only (K27O), K29-only (K29O), K33-only (K33O), K48-only (K48O) and K63-only (K63O) and treated with MG-132 (20 μM) for 6 h. **g** HIF-1α ubiquitination in HEK293T cells transfected with Myc-*HIF-1α* and HA-*MYLIP*, in the presence of wild-type (WT) His-tagged ubiquitin, or the mutant ubiquitins, including K27-only (K27O), K27R mutant ubiquitin (K27R), and treated with MG-132 (20 μM) for 6 h. **h** Endogenous wild-type, K27-linked, K48-linked and K63-linked ubiquitination of HIF-1α in *MYLIP*$^{+/+}$ or *MYLIP*$^{-/-}$ A549 cells under hypoxia (1% O_2) for 4 h. **i** Structure prediction of human HIF-1α protein. **j** Western blot analysis of the indicated proteins in HEK293T cells transfected with HA-empty or HA-*MYLIP* together with Myc-*HIF-1α*-WT or its mutant (K118/442 R). **k** HIF-1α ubiquitination in HEK293T cells transfected with Myc-*HIF-1α*-WT, K118R, K442R or K118/442R and HA-*MYLIP*, in the presence of K27-only (K27O) ubiquitin and treated with MG-132 (20 μM) for 6 h. Data in (**a**–**h**, **j**, **k**) are representative of three independent experiments.

cells under hypoxia (Supplementary Fig. 13c). K117 is localized inside the HIF-2α protein (Supplementary Fig. 13e). Overexpression of *MYLIP* did not induce the degradation of the HIF-2α mutant, K117R (Supplementary Fig. 13f).

We confirmed that *MYLIP* catalyzed the K27-linked polyubiquitination of HIF-2α and that K117 of HIF-2α was the target site of MYLIP (Supplementary Fig. 13g, h). Consistently, the expression of a specific downstream target gene of HIF-2α, *CITED2*, was dramatically promoted in *MYLIP*$^{-/-}$ A549 cells compared to that in *MYLIP*$^{+/+}$ A549 cells under hypoxia (Supplementary Fig. 13i). Furthermore, overexpression of *MYLIP* in H1299 cells significantly suppressed *CITED2* expression under hypoxia (Supplementary Fig. 13j).

Taken together, these data suggest that similar to its effect on HIF-1α, MYLIP also targets HIF-2α to induce its degradation, resulting in the inhibition of HIF-2α activity.

Disruption of *Mylip* in mice promotes hypoxia tolerance

We then generated *Mylip*-deficient mice to study the physiological role of *Mylip* in a mammalian model (Supplementary Fig. 14a–c). Similar to the fish model, no obvious abnormal phenotypes were observed in *Mylip*$^{-/-}$

mice. When *Mylip*$^{+/+}$ and *Mylip*$^{-/-}$ mice of the same age and weight were placed in a hypoxia station (10% O_2) for 2.5 to 3.0 hours, *Mylip*$^{+/+}$ mice began to jump to the top of the gauze-sealed flask, where the mice attempted to get more oxygen through the seal (Fig. 6a; Supplementary Video 3 and 4). However, *Mylip*$^{-/-}$ mice behaved more calmly (Fig. 6a; Supplementary Video 3 and 4). These phenomena suggest that *Mylip*$^{+/+}$ mice are more sensitive to low oxygen (hypoxia). Furthermore, measurement of EPO in mouse serum showed that EPO levels were higher in *Mylip*$^{-/-}$ mice than in *Mylip*$^{+/+}$ mice after hypoxia treatment (Fig. 6b), suggesting that the hypoxia signaling is enhanced in *Mylip*$^{-/-}$ mice compared to *Mylip*$^{+/+}$ mice.

We further confirmed that the HIF-1α and HIF-2α protein levels were higher in *Mylip*$^{-/-}$ than in *Mylip*$^{+/+}$ MEF cells after hypoxia treatment (Fig. 6c). Consistently, endogenous K27-linked polyubiquitination of HIF-1α was lower in *Mylip*$^{-/-}$ than in *Mylip*$^{+/+}$ MEF cells under hypoxia (Fig. 6d).

As expected, the expression of hypoxia-inducible genes, such as *Glut1*, *Vegfa*, *Sod2, Epo*, and *Pgk1*, was increased in *Mylip*$^{-/-}$ MEF cells, mouse brain, kidney, lung, and liver compared to those in *Mylip*$^{+/+}$ mice after hypoxia treatment (Fig. 6e–i).

These data suggest that disruption of *Mylip* in mice results in enhancement of hypoxia signaling and promotion of hypoxia tolerance.

Fish *mylipb* behaves similarly to mammalian *MYLIP* to catalyze the polyubiquitination of hif-α and induce hif-α proteasomal degradation, resulting in the inhibition of hypoxia signaling

We then asked whether fish *mylipb* exerts its function by a mechanism similar to that of mammalian *MYLIP*. The active site of the enzyme in MYLIP is evolutionarily conserved between fish and mammals (Fig. 7a). Overexpression of wild-type zebrafish *mylipb*, but not the enzyme-deficient mutant, mylipb-C/S suppressed the zebrafish hif1αa and hif1αb-induced activity of the HRE-driven luciferase reporter in a dose-dependent manner (Fig. 7b, c; Supplementary Fig. 15a, b). Overexpression of wild-type zebrafish *mylipb*, but not the enzyme-deficient mutant, mylipb-C/S induced degradation of zebrafish hif1-αa and hif1-αb, which was blocked by the addition of MG-132 (Fig. 7d–g; Supplementary Fig. 15c–f; Supplementary Fig. 16a–d).

As expected, wild-type zebrafish *mylipb*, but not the enzyme-deficient mutant, mylipb-C/S, catalyzed the polyubiquitination of zebrafish hif1-αa and hif1-αb (Fig. 7h, i). Consistently, overexpression of wild-type zebrafish *mylipb*, but not the enzyme-deficient mutant, mylipb-C/S significantly suppressed the expression of hypoxia-inducible genes, such as *phd3, glut1, vegfa*, *ldha*, or *cited2* in ZFL cells under hypoxia or with FG4592 treatment (Fig. 7j; Supplementary Fig. 16e–g).

We then examined the effect of zebrafish *mylipb* on zebrafish hif-2αa and hif-2αb. Zebrafish mylipb could bind to and induce the degradation of both hif2αa and hif-2αb (Supplementary Fig. 17a–c). Addition of MG-132 blocked hif-2αa and hif-2αb degradation induced by mylipb (Supplementary Fig. 17d, e). Wild-type zebrafish *mylipb*, but not the enzyme-deficient mutant, mylipb-C/S, catalyzed the polyubiquitination of zebrafish hif2αa and hif-2αb (Supplementary Fig. 17f, g). Consistently, overexpression of wild-type zebrafish *mylipb*, but not the enzyme-deficient mutant, mylipb-C/S, significantly suppressed the zebrafish hif2-αa- and hif-2αb-induced activity of the HRE-driven luciferase reporter (Supplementary Fig. 17h, i). Furthermore, overexpression of wild-type zebrafish *mylipb*, but not the enzyme-deficient mutant, mylipb-C/S, dramatically inhibited the expression of the hypoxia-inducible genes, *cited2,* and *sod2*, in ZFL cells under hypoxia (Supplementary Fig. 17j, k).

Next, we also primarily investigated the mechanism of *M. amblycephala mylipb* in regulating hif-α proteins. *M. amblycephala mylipb* was able to bind to all four *M. amblycephala* hif-α proteins, including hif-1αa, hif-1αb, hif-2αa, and hif-2αb (Supplementary Fig. 18a–d). Notably, overexpression of *M. amblycephala mylipb* resulted in the degradation of *M. amblycephala* hif-1αa, hif-1αb, and hif-2αb, but not of hif-2αa, somewhat different from the effect of zebrafish *mylipb* on zebrafish hif-α proteins (Supplementary Fig. 18e–h). As expected, overexpression of *M. amblycephala mylipb* suppressed the activity of the hypoxia-induced HRE luciferase reporter in a dose-dependent manner (Supplementary Fig 18i). Consistently, overexpression of *M. amblycephala mylipb* significantly inhibited the activity of the HRE luciferase reporter induced by hif-1αa, hif-1αb, and hif-2αb, but not by hif-2αa (Supplementary Fig. 18j–m).

Notably, disruption of *Mylip* in either mice or zebrafish did not affect body weight or length under normal conditions, suggesting that *Mylip* may not affect overall gross phenotypes (Supplementary Fig. S19a–c).

Based on the data obtained in this study, we propose a working model for the role of MYLIP in regulating hypoxia signaling (Supplementary Fig. 20). Under hypoxia, MYLIP is induced and binds to HIF-α to catalyze K27-linked polyubiquitination at lysine 118 and lysine 442 of HIF-1α or lysine 117 of HIF-2α, leading to proteasomal degradation of HIF-α. As a result, hypoxia signaling is attenuated. Disruption of MYLIP in fish and mice promotes hypoxia tolerance.

Discussion

Promoting hypoxia tolerance in aquaculture fish is an important goal in the modern aquaculture industry, not only to increase the yield per unit of water, thus saving farming costs and avoiding water pollution from aquaculture effluents, but also to improve fish health[41]. However, how to achieve this goal is still a major challenge. To date, it is known that the hypoxia adaptation in humans, terrestrial animals, and fish, is mainly controlled by the hypoxia signaling pathway[2,42–44]. In fact, several different types of hypoxia-adaptive mutations have been identified in HIF-1α, HIF-2α, and PHD2[45–47]. It is still controversial how enhancement or inhibition of this pathway affects hypoxia tolerance or adaptation. It seems that most of the time, enhancement of the hypoxia signaling pathway benefits hypoxia tolerance[35–37,48], but sometimes it also seems that the inhibition of the hypoxia signaling pathway promotes hypoxia tolerance[38]. Therefore, maintaining the homeostasis of the hypoxia signaling may be beneficial for animals to reduce the damage caused by hypoxic conditions. In this study, based on our previous experience, we performed the screening of hypoxia-induced E3 ubiquitin ligases in *M. amblycephala* and fortunately identified a repressor of the hypoxia signaling pathway, *mylipb*. Disruption of *mylipb* in fish resulted in the upregulation of hypoxia signaling, leading to the improvement of hypoxia tolerance in fish. This study may provide a clue for identifying targets for breeding fish strains with hypoxia tolerance, which will benefit the aquaculture industry.

It is well defined that the degradation of HIF-α under normoxia is mainly mediated by the PHD-pVHL pathway[5,40,49]. How the stability of HIF-α proteins is controlled under hypoxia is still poorly understood. As a major mechanism for controlling protein stability, ubiquitination mediated by E3 ligases and deubiquitination mediated by deubiquitinases have been shown to directly or indirectly control HIF-α abundance under normoxia or hypoxia[9,50–54]. As one of the seven major types of polyubiquitination, K27-linked polyubiquitination usually affects its targets in activation, trafficking, processing, aggregation, etc., and rarely mediates the degradation of its targets as does K48-linked polyubiquitination[55–57]. Here, we found that MYLIP targets HIF-α to catalyze K27-linked polyubiquitination at K118/442 or K117, leading to proteasomal degradation, revealing a novel modification to control HIF-α stability under hypoxia. Notably, K442 is not as conserved as K118 in HIF-1α, and its homologous site cannot be found in HIF-2α. Perhaps this is why only MYLIP target site (K117) has been identified in HIF-2α. Fish typically have multiple copies of a homologous gene due to genome duplication during evolution. Zebrafish and *M. amblycephala* have two HIF-1α genes, hif-1αa and hif-1αb, and two HIF-2α genes, hif-2αa and hif-2αb. Interestingly, the effect of *mylipb* on these four genes appears to be quite different. Zebrafish *mylipb* targets hif-1αa, hif-1αb, hif-2αa, and hif-2αb for degradation, and *M. amblycephala mylipb* targets hif-1αa, hif-1αb, and hif-2αb but not hif-2αa for degradation. These data suggest that the function of fish HIF-α is likely to be differentially altered in the regulation of hypoxia signaling.

To date, only LDLR, VLDLR and APOER2 have been identified as targets of MYLIP[29,31–33]. Because all of these genes are related to lipoprotein metabolism and are so narrowly targeted, it is hypothesized that *MYLIP*

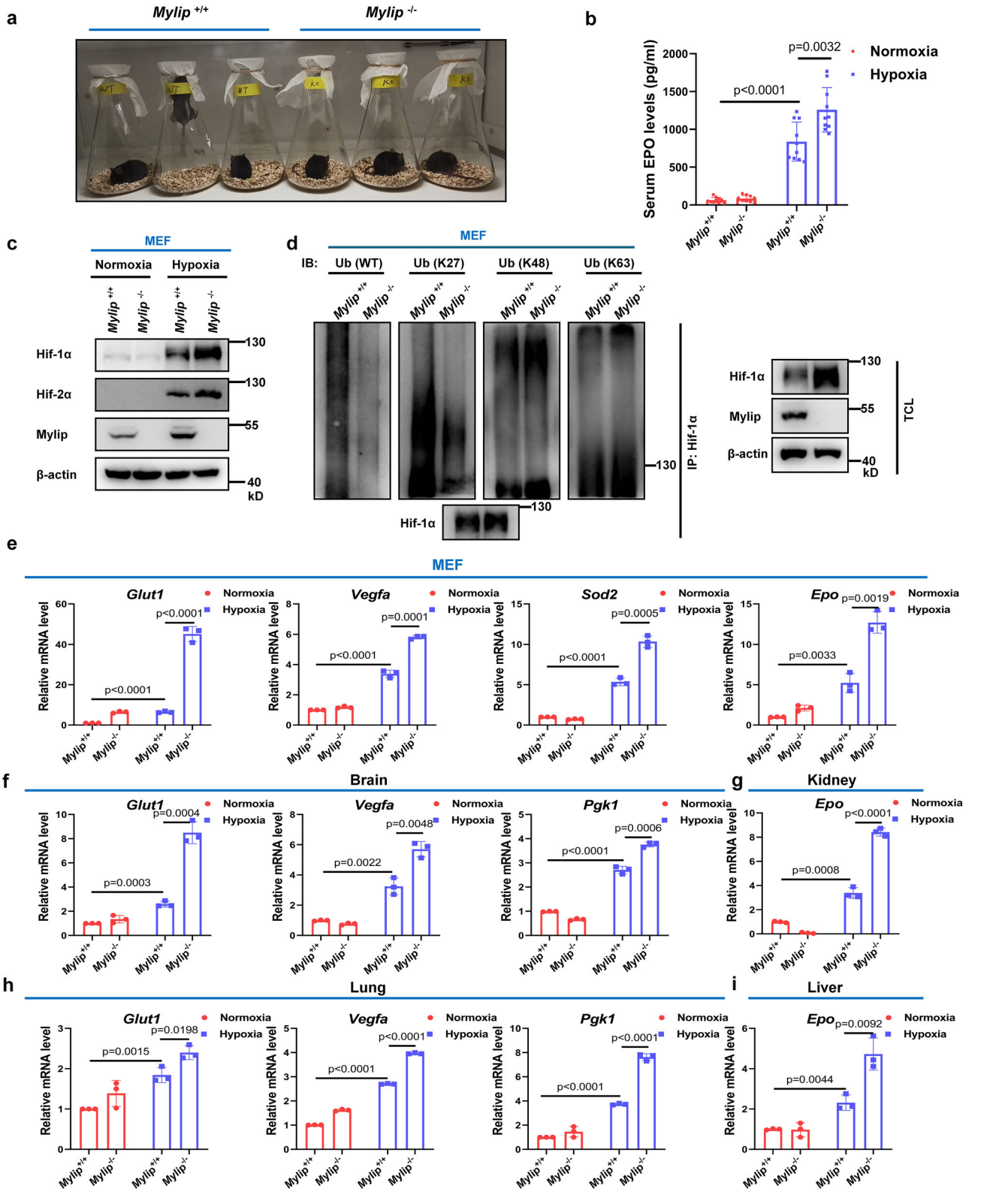

Fig. 6 | Disruption of *Mylip* in mice promotes hypoxia tolerance by enhancing hypoxia signaling. a Images of *Mylip*$^{+/+}$ and *Mylip*$^{-/-}$ mice (7 weeks) under hypoxia (10% O_2) for 3 h. **b** ELISA of Epo in serum from *Mylip*$^{+/+}$ and *Mylip*$^{-/-}$ mice ($n = 10$ per group) under hypoxia (10% O_2) for 3 h. **c** Western blot analysis of the indicated proteins in *Mylip*$^{+/+}$ or *Mylip*$^{-/-}$ MEF cells under normoxia (21% O_2) or hypoxia (1% O_2) for 4 h. **d** Endogenous wild-type, K27-linked, K48-linked and K63-linked ubiquitination of Hif-1α in *Mylip*$^{+/+}$ or *Mylip*$^{-/-}$ MEF cells under hypoxia (1% O_2) for 4 h. **e** qPCR analysis of *Glut1, Vegfa, Sod2, Epo* mRNA in *Mylip*$^{+/+}$ or *Mylip*$^{-/-}$ MEF cells under normoxia (21% O_2) or hypoxia (1% O_2) for 18 h. **f** qPCR analysis of *Glut1, Vegfa, Pgk1* mRNA in the brain of *Mylip*$^{+/+}$ or *Mylip*$^{-/-}$ mice under hypoxia (10% O_2) for 3 h. **g** qPCR analysis of *Epo* mRNA in the kidney of *Mylip*$^{+/+}$ or *Mylip*$^{-/-}$ mice under hypoxia (10% O_2) for 3 h. **h** qPCR analysis of *Glut1, Vegfa, Pgk1* mRNA in the lung of *Mylip*$^{+/+}$ or *Mylip*$^{-/-}$ mice under hypoxia (10% O_2) for 3 h. **i** qPCR analysis of *Epo* mRNA in the liver of *Mylip*$^{+/+}$ or *Mylip*$^{-/-}$ mice under hypoxia (10% O_2) for 3 h. Data in (**c**, **d**) are representative of three independent experiments. Data in (**e**–**i**) are presented as mean ± S.D., two-tailed Student's *t* test; $n = 3$ biologically independent experiments.

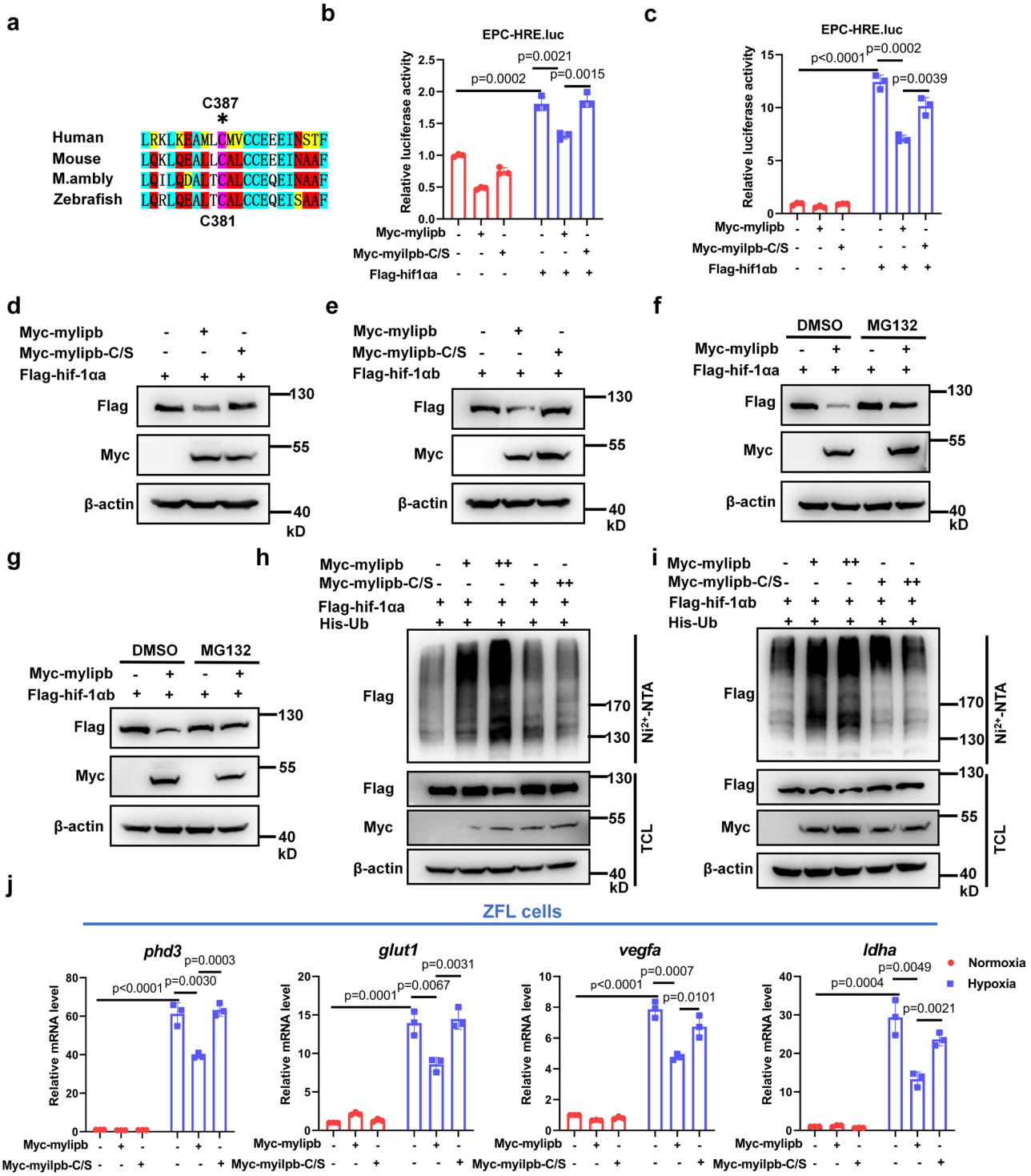

Fig. 7 | Zebrafish mylipb promotes hif-1α degradation and inhibits hif-1α activity depending on its enzymatic activity. a The enzyme active sites in MYLIP of human, mouse, bluntsnout bream, and zebrafish. **b**, **c** The effects of mylipb or its enzyme-deficient mutant (C381S) on the transcriptional activity of hif1αa (**b**) and hif1αb (**c**) as measured by HRE luciferase reporter activity in EPC cells. **d**, **e** Western blot analysis of the indicated proteins in HEK293T cells transfected with Flag-*hif-1αa* (**d**), Flag-*hif-1αb* (**e**) together with Myc-*mylipb* or Myc-*mylipb*-C/S. **f**, **g** Western blot analysis of the indicated proteins in HEK293T cells transfected with Flag-*hif-1αa* (**f**), Flag-*hif-1αb* (**g**) together with Myc-*mylipb* and treated with MG-132 (20 μM) for 6 h. **h**, **i** Hif-1αa (**h**) and hif-1αb (**i**) ubiquitination in HEK293T cells transfected with Flag-*hif-1αa* (**h**) or Flag-*hif-1αb* (**i**) and Myc-*mylipb* or Myc-*mylipb*-C/S, in the presence of His-tagged wild-type (WT) ubiquitin and treated with MG-132 (20 μM) for 6 hours. **j** qRT-PCR analysis of *phd3*, *glut1*, *vegfa*, and *ldha* mRNA in ZFL cells transfected with Myc empty, Myc-*mylipb*, or Myc-*mylipb*-C/S under normoxia (21% O_2) or hypoxia (1% O_2) for 18 h. Data in (**b**, **c**, **j**) are presented as mean ± S.D., two-tailed Student's *t* test; *n* = 3 biologically independent experiments. Data in (**d**–**i**) are representative of three independent experiments.

may behave in a rather unique manner, in contrast to most E3 ubiquitin ligases, which are promiscuous and have a broader spectrum of ubiquitination targets[58]. In this study, we identified additional targets of MYLIP, HIF-1α, and HIF-2α, involved in hypoxia signaling, suggesting that MYLIP may have other functions in the regulation of lipoprotein metabolism than previously thought. In particular, the FERM domain is known to mediate the interaction between membranes and membrane proteins[59] and may also serve as the key domain for binding to lipoprotein receptors. However, HIF-1α binds to the RING domain instead of the FERM domain, further suggesting that HIF-1α/2α serve as a different type of target for MYLIP. However, it remains a mystery why a lipoprotein metabolism-related E3 ligase regulates hypoxia signaling. Further elucidation of the underlying mechanisms may help to understand the relationship between the hypoxia signaling pathway and lipoprotein metabolism.

Because they belong to the same family of transcription factors, HIF-1α and HIF-2α share most of the downstream targets, but they also have their own specific downstream targets[40]. In this study, we identified *MYLIP* as a specific downstream target of HIF-2α, but not of HIF-1α. However, MYLIP can modulate both HIF-1α and HIF-2α by inducing their K27-linked polyubiquitination and subsequent proteasomal degradation, revealing an interesting negative feedback regulatory loop of hypoxia signaling.

Methods

Ethics statement

The laboratory animal facility was accredited by the Association for Assessment and Accreditation of Laboratory Animal Care International (AAALAC), and all the animal procedures used in this study were approved by the Institutional Animal Care and Use Committee (IACUC) of the Institute of Hydrobiology, Chinese Academy of Sciences.

Reagents and antibodies

See Supplementary Table 1.

Mice

Mylip$^{+/-}$ mice on the C57BL/6 background were purchased from the Cyagen Biosciences (https://www.cyagen.com/cn/zh-cn/sperm-bank/71974). Mice were maintained in isolated, ventilated cages (maximum of five mice per cage) in a barrier facility on a 12/12-hour light/dark cycle, 22–26 °C, with unrestricted access to standard chow and tap water. Six- to eight-week-old mice were used in the experiments. Same-sex littermates were randomly assigned to the experimental groups.

Zebrafish

Zebrafish strain AB and the transgenic line Tg(gata1:EGFP) (provided by Tingxi Liu, Shanghai Institutes for Biological Sciences, Chinese Academy of Sciences, China) were bred, maintained, and staged according to standard protocols. The *mylipb*-null zebrafish line, *mylipb*$^{ihbmb73/ihbmb73}$(https://zfin.org/ZDB-ALT-230809-2), was generated by CRISPR/Cas9-mediated mutagenesis. The procedure for generating *mylipb*-null zebrafish has been described previously[39,50]. All zebrafish experiments were approved by the Institutional Animal Care and Use Committee of the Institute of Hydrobiology, Chinese Academy of Sciences.

Bluntsnout bream (*M. amblycephala*)

The parents of bluntsnout bream (*M. amblycephala*) were obtained from Dr. Zexia Gao's laboratory of Huazhong Agricultural University. CRISPR/Cas9 technology was used for gene editing of *mylipb* in *M. amblycephala*. *M. amblycephala mylipb* single guide RNA (sgRNA) was synthesized using a TranscriptAid T7 High Yield Transcription Kit (Thermo Scientific). *M. amblycephala* one-cell stage embryos were injected with 2 pg of Cas9 protein and 0.3 pg of sgRNA per embryo. The Heteroduplex Mobility Assay (HMA) was used to confirm mutation detection in injected embryos. If the HMA results were positive, the remaining embryos were treated as F0 and grown to maturity. The F0 *M. amblycephala* were then backcrossed to wild-type (WT) *M.* amblycephala to generate F1. The F1 heterozygotes were also genotyped by HMA and further confirmed by sequencing the PCR fragments containing the target sites. *M. amblycephala mylipb* heterozygous and wild-type siblings were reared in 120 × 100 × 45 cm^3 tanks with continuous freshwater aeration under fluorescent lamps light from 8:00 am to 8:00 pm. Temperature conditions were maintained at 25.0 ± 1.0 °C at the Aquaculture Laboratory, Chinese Academy of Sciences (Wuhan, China). All experiments with *M. amblycephala* were approved by the Institutional Animal Care and Use Committee of the Institute of Hydrobiology, Chinese Academy of Sciences (IHB-2022–039).

Screening of hypoxia-induced E3 ubiquitin ligases by transcriptome analysis

M. amblycephala (2 mpf) of similar weight were selected for hypoxia experiments. The flask was filled with 200 ml of water. Three *M. amblycephala* were placed in a flask under normoxia (21% O_2) or hypoxia (5% O_2) for 2 hours. The above-sampled fish were euthanized by a concentration of 0.3mg/L MS-222, and the brain was dissected and immediately stored in liquid nitrogen for total RNA extraction. The experiments were repeated five times ($n = 5$ per group). Clustering of indexed samples was performed on a cBot cluster generation system using the TruSeq PE Cluster Kit v4-cBot-HS (Illumia) according to the manufacturer's instructions. After cluster generation, the library preparations were sequenced on an Illumina Hiseq 4000 platform, and paired-end 150 bp reads were generated. Differential expression analysis of two conditions/groups was performed using the DESeq R package (1.10.1). DESeq provides statistical routines to determine differential expression in digital gene expression data using a model based on the negative binomial distribution. The resulting *P* values were adjusted using Benjamini and Hochberg's approach to control for the false discovery rate. Genes with an adjusted *P* value < 0.05 found by DESeq were considered to be differentially expressed. All the differentially expressed E3 ubiquitin ligases were selected for hypoxia-induced E3 ubiquitin ligases.

Cell culture

Zebrafish liver (ZFL) cells originally obtained from the American Type Culture Collection (ATCC) were cultured in Ham's F-12 medium (HyClone) supplemented with 10% fetal bovine serum (FBS) (Biological Industries). Epithelioma papulosum cyprini (EPC) cells, originally obtained from the ATCC, were cultured in Earle's Medium 199 (Biological Industries) supplemented with 10% FBS. ZFL and EPC cells were maintained at 28 °C in a humidified incubator containing 5% carbon dioxide (CO_2). HEK293T, H1299, and A549 cells, originally obtained from ATCC were cultured in Dulbeccos' modified Eagle's medium (DMEM) (HyClone) supplemented with 10% FBS. Primary mouse embryonic fibroblasts (MEFs) were prepared from embryos at 12.5–14.5 days embryos and cultured in DMEM containing 10% FBS and 1% streptomycin-penicillin. HEK293T, H1299, A549, and MEF cells were maintained at 37 °C in a humidified incubator containing 5% CO_2.

Luciferase reporter assay

Cells seeded in 24-well plates were transfected with the indicated plasmids together with pCMV-Renilla as an internal control. After transfection for 24 hours, luciferase activity was quantified using the dual-luciferase reporter assay system (#E1960, Promega). The data were normalized to Renilla luciferase. Three independent experiments were performed, and the mean ± SD of three replicate experiments was used for statistical analysis.

Quantitative real-time PCR

Total RNA was extracted using RNAiso Plus (TaKaRa Bio., Beijing, China) according to the manufacturer's protocol. cDNA was synthesized using Revert Aid First Strand cDNA Synthesis Kit (Thermo Scientific, Waltham, MA, USA). MonAmpTM SYBR® Green qPCR Mix (high Rox) (Monad Bio., Shanghai, China) was used for quantitative RT-PCR assays (qPCR). Primers for quantitative RT-PCR assays are listed in Supplementary Table 2.

Construction of the MYLIP promoter luciferase reporter

The *MYLIP* promoter (position −541 to −5) for its luciferase reporter construct was amplified from total DNA extracted from HEK293T cells by PCR using primers 5'-TTTCTCTATCGATAGGTACCTTTGCCAGGC TGGTCTCGAATCTGACCT-3' and 5'-CTTAGATCGCAGATCTCGA GCGCTGCGACAGGGACTCTGCTGATATA-3'. The promoter reporter mut1 was constructed by mutating GCGTG (position −468 to −463) to AAATG. Promoter reporter mut2 was constructed by mutating GCGTG (position −385 to −380) to AAATG. Promoter reporter mut1/2 was constructed by simultaneously mutating both GCGTG (position −385 to −380) and GCGTG (position −468 to −463) to AAATG. These four promoters were then subcloned into the pGL3-Basic vector (Clontech).

Chromatin immunoprecipitation assay

A549 cells were cross-linked with 1% formaldehyde for 10 mins at 37 °C and quenched in 0.125 M glycine. DNA was immunoprecipitated from the sonicated cell lysates and quantified by SYBR Green real-time PCR analysis (Bio-Rad). Primer sequences are listed in supplementary Table S2. Fold enrichment was calculated based on Ct as $2-\Delta(\Delta Ct)$, where $\Delta Ct = CtIP–CtInput$ and $\Delta(\Delta Ct) = \Delta Ctantibody - \Delta CtIgG$. LDHA, a specific downstream target of HIF-1α, but not of HIF-2α, was selected as a control. Primers for the promoter of LDHA were described previously 60. The primers specific for the MYLIP promoter region from position −458 to −257 were 5'-ACCATGCCCGGACGAGAACA-3' (forward) and 5'-gctgctcagagtgagcgatc-3' (reverse). The primers (control) for the MYLIP promoter region from position -1372 to −1149, far from MYLIP binding sites, were 5'-tgctgggattacaggtgtgagc-3' (forward) and 5'-GGTCAGG AGATGAGCACCTTACC-3' (reverse).

GST pull-down

GST-tagged HIF-1α and His-tagged MYLIP were expressed in *Escherichia coli* (BL21). Monoclonal colonies expressing the target protein were picked and inoculated into 5 mL LB medium containing ampicillin and cultured overnight at 37 °C. The culture was then inoculated into fresh Amp-containing LB medium at a ratio of 1:20 and continuously cultured at 37 °C until the OD600 of the bacterial culture reached 0.5–0.7. IPTG was added to a final concentration of 1 mM to induce protein expression at 37 °C for 2–4 hours. Bacterial cultures were collected in centrifuge tubes and purified using GST-tag protein purification kit (Beyotime, P2262) and His-tag protein purification kit (Beyotime, P2229S) according to the manufacturer's instructions. GST (1 μg) or GST-HIF-1α (1 μg) was incubated with His-MYLIP (1 μg) overnight (4 °C). The association of GST-HIF-1α with His-MYLIP was detected by immunoblotting with anti-HIF-1α and anti-His antibodies. GST and GST-HIF-1α proteins were stained with Coomassie Blue.

In vitro ubiquitinylation assay

The in vitro ubiquitinylation assay was performed using the Enzo Ubiquitinylation Kit (BML-UW9920-0001) according to the manufacturer's instructions. Briefly, purified GST-HIF-1α was mixed with purified E3 ligases His-MYLIP together with E1, E2 (UbcH5a, UbcH5b, UbcH5c), ubiquitin, ATP, and reaction buffer provided in the kit. The reaction was processed by incubation at 37 °C for 30 min, denatured by addition of SDS-containing loading buffer, boiled at 100 °C for 5 min, separated by SDS-PAGE, and transferred to a PVDF membrane. An anti-HIF-1α antibody was used to detect ubiquitylation patterns on substrate proteins by immunoblotting.

CRISPR-Cas9 knockout cell lines

To generate A549 knockout cell lines of the indicated genes, sgRNA sequence was ligated into Lenti-CRISPRv2 plasmid and then co-transfected with viral packaging plasmids (psPAX2 and pMD2G) into HEK293T cells. Six hours after transfection, the medium was changed, and the viral supernatant was collected and filtered through a 0.45 μm screen. Targeted cells were infected with viral supernatant and selected with 1 μg/ml puromycin for 2 weeks. The VHL-targeting sgRNA sequence was described as previously[60,61]. The MYLIP targeting sgRNA sequence is: CACCGGTAGCAAAGGTGAAAGTTTA.

Immunoprecipitation assay and western blot analysis

For co-immunoprecipitation and western blot analysis, cells were briefly lysed in 1 mL RIPA buffer containing 50 mM Tris (pH 7.4), 1% Nonidet P-40, 0.25% sodium deoxycholate, 1 mM EDTA (pH 8.0), 150 mM NaCl, 1 mM NaF, 1 mM PMSF, 1 mM Na3VO4, and a 1:100 dilution of protease inhibitor mixture for 30 min at 4 °C. After centrifugation at 12,000 × *g* for 15 min, protein concentrations were measured, and equal amounts of lysates were used for immunoprecipitation. Immunoprecipitation was performed with the indicated beads or with different antibodies and Protein A-Sepharose overnight at 4 °C. The precipitates were then washed three times with RIPA buffer, and the immunocomplexes were eluted with sample buffer containing 1% SDS for 5 minutes at 95 °C. The immunoprecipitated proteins were separated by SDS-PAGE. Western blot analysis was performed with the specific antibodies and horseradish peroxidase (HRP)-conjugated anti-mouse or anti-rabbit secondary antibodies. The Fuji Film LAS4000 mini-luminescence image analyzer was used to photograph the blots. ImageJ software was used to quantify protein levels based on the band density obtained by Western blot analysis.

Nucleus and cytoplasm separation

Nuclear and cytoplasmic separation was performed using the Nuclear and Cytoplasmic Extraction Kit (#78833, Thermo Scientific) according to the manufacturer's protocol. The extracts were analyzed by western blot analysis. To ensure the efficiency of fraction separation, anti-α-tubulin antibody was used to monitor cytoplasmic proteins, and anti-histone H3 antibody was used to monitor nuclear proteins.

Ubiquitination assay

Ubiquitination assays were performed according to the previously described method with some modifications[50]. Briefly, HEK293T cells were co-transfected with the plasmids expressing Myc-*HIF-1α*, His-ubiquitin or His-ubiquitin-K48 or His-ubiquitin-K48R, together with Myc-*MYLIP* or Myc empty as a control for 24 h and then lysed by denatured buffer (6 M guanidine-HCl, 0.1 M Na_2HPO_4/NaH_2PO_4, 10 mM imidazole), followed by nickel bead purification and immunoblotting with the indicated antibodies. For ubiquitination assay in *MYLIP* $^{+/+}$ or *MYLIP*$^{-/-}$ A549 cells, the cells were cultured under hypoxia (1% O_2), then harvested and lysed with the lysis buffer (100 μl). The supernatants were denatured at 95 °C for 5 minutes in the presence of 1% SDS. The denatured lysates were diluted with lysis buffer to reduce the concentration of SDS (<0.1%). Immunoprecipitation (denature-IP) was performed with anti-HIF-1α antibody, followed by immunoblotting with anti-ubiquitin or anti-K27-linkage-specific polyubiquitin antibody.

Immunofluorescence confocal microscopy

Cells grown on glass coverslips were fixed with 4% paraformaldehyde in PBS for 20 minutes, permeabilized with 0.1% Triton X-100, and blocked with 1% bovine serum albumin. Cells were then stained with the indicated primary antibodies (anti-HIF-1α, 1:1000, Cell Signaling Technology) followed by incubation with fluorescent dye-conjugated secondary antibodies. Cell nuclei were counterstained with DAPI (Thermo Fisher). Cell imaging was performed with a Leica laser scanning confocal microscope.

ELISA

The concentration of mouse Epo in serum was measured using commercially available ELISA kits (Promoter) according to the manufacturer's instructions. The concentration of lactic acid in cells was measured with commercial kits (biobox) according to the manufacturer's instructions.

O-dianisidine staining

The *mylipb*$^{+/+}$ and *mylipb*$^{-/-}$ zebrafish larvae [36 hours post-fertilization (hpf); $n = 10$] were incubated in disposable 60-mm cell culture dishes filled

with 5 mL of egg water were incubated under normoxic and hypoxic conditions for 10 hours. The larvae were then incubated with *O*-dianisidine solution (Sigma-Aldrich *O*-dianisidine dissolved in 100% ethanol, 0.1 M sodium acetate, and 30% H_2O_2) in a 12-well plate for 1 hour. After incubation, the larvae were washed with ddH2O and fixed with 4% paraformaldehyde in PBS at 4 °C overnight. The larvae were then incubated in a bleaching solution (0.9% H_2O_2, 0.8% KOH, and 0.1% Tween in ddH_2O) for 30 minutes to remove their natural pigmentation, and then in 4% paraformaldehyde for further fixation. After these steps, the larvae were immersed in 3% methylcellulose M450 solution in a 100 mm cell culture dish and imaged using a Nikon TE2000-U microscope. IpWin32 software was used to quantify the number of erythrocytes and GFP-positive cells. Cell numbers were measured from the field of view with an equal square, and different larvae were selected for counting.

Sequence alignment and phylogenetic analysis

The amino acid sequences of mylipb and HIF-1α were downloaded from the National Center for Biotechnology Information (https://www.ncbi.nlm.nih.gov) and compared using MEGA 7.0 software. The similarity between different MYLIP proteins was calculated using the Clustalw program. The multiplex alignment of MYLIP proteins was constructed by using MEGA 7.0 software based on the neighbor-joining (NJ) method with 1000 bootstrap replicates. SWISS-MODEL (https://swissmodel.expasy.org/) was used to predict the protein structure.

Hypoxia treatment

The Ruskinn INVIVO2 I-400 workstation was used for hypoxia treatment of cells, zebrafish, *M. amblycephala, and mice*. Prior to use, the O_2 concentration was pre-adjusted to the indicated values ahead of time. The O_2 concentration and temperature were pre-adjusted in advance to the corresponding values (1% O_2, 28 °C for ZFL and EPC cells, 1% O_2, 37 °C for HEK293T, A549, H1299 and MEF cells, 2% O_2 or 10% O_2, 28 °C for zebrafish larvae, 5% O_2, 28 °C for adult zebrafish, 10% O_2, 28 °C for *M. amblycephala* and 10% O_2, 26 °C for mouse) ahead of time. For cell hypoxia treatment, ZFL or EPC cells were cultured in the hypoxia workstation for 18 h, HEK293T, A549, H1299, or MEF cells were cultured in the hypoxia workstation for 4 hours or 18 hours. For the experimental animals, those with normal growth and development were selected and randomly divided into two groups of equal numbers: one serving as a normoxic control group and the other subjected to hypoxic treatment. For hypoxia treatment on zebrafish larvae (3 dpf), $mylipb^{+/+}$ and $mylipb^{-/-}$ zebrafish larvae ($n = 50$) were simultaneously plated in 60-mm disposable cell culture dishes filled with 5 ml egg water and were plated in the hypoxia workstation. The behavior of the zebrafish was then closely monitored, recorded, and photographed. To obtain the survival curve of zebrafish under hypoxia, mortality was monitored every 1 hour after the first death, We identified dead larvae based on characteristics such as no movement, no blood circulation, and a degenerated body. For hypoxia treatment of zebrafish larvae (36 hpf or 48 hpf), $mylipb^{+/+}$ and $mylipb^{-/-}$ zebrafish larvae ($n = 30$) were simultaneously plated in 60-mm disposable cell culture dishes filled with 5 ml egg water in the hypoxia workstation for 10 hours. For hypoxia treatment of the adult zebrafish (3 mpf), zebrafish of similar weight were selected for further experiments. Two flasks were filled with 250 mL of water. Three $mylipb^{+/+}$ were added to one flask, and three $mylipb^{-/-}$ were added to the other. After the flasks containing zebrafish were placed in the hypoxia workstation, the behavior of the zebrafish was closely observed, recorded, and photographed. To obtain the survival curve of zebrafish under hypoxia, mortality was monitored every 0.5 hours after the first death. For hypoxia treatment on *M. amblycephala* (3 mpf), *M. amblycephala* of similar weight were used. Two flasks were filled with 400 mL of water. Three $mylipb^{+/+}$ were placed in one flask and three $mylipb^{+/-}$ in the other. After the flasks containing *M. amblycephala* were placed in the hypoxia workstation, the behavior of the *M. amblycephala* was closely observed, recorded, and photographed. To obtain the survival curve of *M. amblycephala* under hypoxia, mortality was monitored every 0.25 hour after the first death. For hypoxia treatment of adult mice (7 weeks), mice of similar weight were selected for further experiments. Each mouse was placed in one flask. The flasks were sealed with gauze and then placed in the hypoxia workstation. The behavior of the mice in the flasks was closely observed, recorded, photographed, or videotaped. Because it was difficult to obtain mice with different genetic backgrounds (+/+, −/−) but similar body weight at the same time, we used mice from different litters. The experiments were repeated ten times ($n = 10$/each group (+/+, −/−). The total number of mice used in the hypoxia treatment experiments was 20 ($n = 20$). Specimens were harvested sequentially according to the pre-established hypoxic treatment timeline during sampling and analysis. The experimental procedures were not blinded because they were conducted by a single researcher.

Statistics and reproducibility

No statistical methods were used to estimate sample size. Survival data were calculated by the Kaplan–Meier method and analyzed by the Gehan-Breslow-Wilcoxon test using GraphPad Prism 8.0 (GraphPad Software). Other statistical analyses were performed using an unpaired *t* test analysis in GraphPad Prism 8.0 (GraphPad Software). Statistical analyzed data are expressed as mean ± standard deviation (S.D.). A p value < 0.05 was considered statistically significant. Statistical analyses were performed with GraphPad Prism 8.0 (GraphPad Software). Data were derived from three independent reproducible experiments.

Reporting summary

Further information on research design is available in the Nature Portfolio Reporting Summary linked to this article.

Data availability

Uncropped blot images are included as Supplementary Information. The source data behind the graphs in the paper are provided as Supplementary Data 1. The original RNA-seq data were uploaded to the GEO datasets (GSE283363). Any additional information required to reanalyze the data reported in this paper is available from the corresponding author upon request.

Received: 13 January 2025; Accepted: 9 May 2025;
Published online: 21 May 2025

References

1. Gui, J.-F. Chinese wisdom and modern innovation of aquaculture. *Water Biol. Secur.* **3**, 100271 (2024).
2. Xiao, W. The hypoxia signaling pathway and hypoxic adaptation in fishes. *Sci. China Life Sci.* **58**, 148–155 (2015).
3. Lee, F. S. Hypoxia Inducible Factor pathway proteins in high-altitude mammals. *Trends Biochem. Sci.* **49**, 79–92 (2024).
4. Kaelin, W. G. Jr Von Hippel-Lindau disease: insights into oxygen sensing, protein degradation, and cancer. *J. Clin. Invest.* **132**, e162480 (2022).
5. Kaelin, W. G. Jr & Ratcliffe, P. J. Oxygen sensing by metazoans: the central role of the HIF hydroxylase pathway. *Mol. Cell* **30**, 393–402 (2008).
6. Kaelin, W. G. Proline hydroxylation and gene expression. *Annu Rev. Biochem.* **74**, 115–128 (2005).
7. Schofield, C. J. & Ratcliffe, P. J. Oxygen sensing by HIF hydroxylases. *Nat. Rev. Mol. Cell Biol.* **5**, 343–354 (2004).
8. Majmundar, A. J., Wong, W. J. & Simon, M. C. Hypoxia-inducible factors and the response to hypoxic stress. *Mol. Cell* **40**, 294–309 (2010).

9. Kubaichuk, K. & Kietzmann, T. Involvement of E3 Ligases and deubiquitinases in the control of hif-alpha subunit abundance. *Cells* **8**, 598 (2019).
10. Albanese, A., Daly, L. A., Mennerich, D., Kietzmann, T. & See, V. The role of hypoxia-inducible factor post-translational modifications in regulating its localisation, stability, and activity. *Int. J. Mol. Sci.* **22**, 268 (2020).
11. Wu, H. T. et al. K63-polyubiquitinated HAUSP deubiquitinates HIF-1alpha and dictates H3K56 acetylation promoting hypoxia-induced tumour progression. *Nat. Commun.* **7**, 13644 (2016).
12. Bononi, A. et al. BAP1 is a novel regulator of HIF-1alpha. *Proc. Natl. Acad. Sci. USA* **120**, e2217840120 (2023).
13. Lv, C. et al. USP14 maintains HIF1-alpha stabilization via its deubiquitination activity in hepatocellular carcinoma. *Cell Death Dis.* **12**, 803 (2021).
14. Nelson, J. K. et al. USP25 promotes pathological HIF-1-driven metabolic reprogramming and is a potential therapeutic target in pancreatic cancer. *Nat. Commun.* **13**, 2070 (2022).
15. Lim, J. H. et al. Sirtuin 1 modulates cellular responses to hypoxia by deacetylating hypoxia-inducible factor 1alpha. *Mol. Cell* **38**, 864–878 (2010).
16. Dioum, E. M. et al. Regulation of hypoxia-inducible factor 2alpha signaling by the stress-responsive deacetylase sirtuin 1. *Science* **324**, 1289–1293 (2009).
17. Bae, S. H. et al. Sumoylation increases HIF-1alpha stability and its transcriptional activity. *Biochem. Biophys. Res. Commun.* **324**, 394–400 (2004).
18. Berta, M. A., Mazure, N., Hattab, M., Pouyssegur, J. & Brahimi-Horn, M. C. SUMOylation of hypoxia-inducible factor-1alpha reduces its transcriptional activity. *Biochem. Biophys. Res. Commun.* **360**, 646–652 (2007).
19. Cheng, J., Kang, X., Zhang, S. & Yeh, E. T. SUMO-specific protease 1 is essential for stabilization of HIF1alpha during hypoxia. *Cell* **131**, 584–595 (2007).
20. Carbia-Nagashima, A. et al. RSUME, a small RWD-containing protein, enhances SUMO conjugation and stabilizes HIF-1alpha during hypoxia. *Cell* **131**, 309–323 (2007).
21. Mylonis, I. et al. Identification of MAPK phosphorylation sites and their role in the localization and activity of hypoxia-inducible factor-1alpha. *J. Biol. Chem.* **281**, 33095–33106 (2006).
22. Warfel, N. A., Dolloff, N. G., Dicker, D. T., Malysz, J. & El-Deiry, W. S. CDK1 stabilizes HIF-1alpha via direct phosphorylation of Ser668 to promote tumor growth. *Cell Cycle* **12**, 3689–3701 (2013).
23. Kalousi, A. et al. Casein kinase 1 regulates human hypoxia-inducible factor HIF-1. *J. Cell Sci.* **123**, 2976–2986 (2010).
24. Xu, D., Yao, Y., Lu, L., Costa, M. & Dai, W. Plk3 functions as an essential component of the hypoxia regulatory pathway by direct phosphorylation of HIF-1alpha. *J. Biol. Chem.* **285**, 38944–38950 (2010).
25. Geng, H. et al. HDAC4 protein regulates HIF1alpha protein lysine acetylation and cancer cell response to hypoxia. *J. Biol. Chem.* **286**, 38095–38102 (2011).
26. Liu, X. et al. Repression of hypoxia-inducible factor alpha signaling by Set7-mediated methylation. *Nucleic Acids Res.* **43**, 5081–5098 (2015).
27. Montagner, M. et al. SHARP1 suppresses breast cancer metastasis by promoting degradation of hypoxia-inducible factors. *Nature* **487**, 380–384 (2012).
28. Oh, E. T. et al. NQO1 inhibits proteasome-mediated degradation of HIF-1alpha. *Nat. Commun.* **7**, 13593 (2016).
29. Zelcer, N., Hong, C., Boyadjian, R. & Tontonoz, P. LXR regulates cholesterol uptake through Idol-dependent ubiquitination of the LDL receptor. *Science* **325**, 100–104 (2009).
30. Sorrentino, V. & Zelcer, N. Post-transcriptional regulation of lipoprotein receptors by the E3-ubiquitin ligase inducible degrader of the low-density lipoprotein receptor. *Curr. Opin. Lipidol.* **23**, 213–219 (2012).
31. Hong, C. et al. The E3 ubiquitin ligase IDOL induces the degradation of the low density lipoprotein receptor family members VLDLR and ApoER2. *J. Biol. Chem.* **285**, 19720–19726 (2010).
32. Gao, J. et al. The E3 ubiquitin ligase IDOL regulates synaptic ApoER2 levels and is important for plasticity and learning. *Elife* **6**, e29178 (2017).
33. Lee, S. D. et al. IDOL regulates systemic energy balance through control of neuronal VLDLR expression. *Nat. Metab.* **1**, 1089–1100 (2019).
34. Lane-Donovan, C. & Herz, J. The ApoE receptors Vldlr and Apoer2 in central nervous system function and disease. *J. Lipid Res* **58**, 1036–1043 (2017).
35. Liao, Q. et al. Disruption of sirtuin 7 in zebrafish facilitates hypoxia tolerance. *J. Biol. Chem.* **299**, 105074 (2023).
36. Liao, Q. et al. Deletion of prolyl hydroxylase domain-containing enzyme 3 (phd3) in zebrafish facilitates hypoxia tolerance. *J. Biol. Chem.* **299**, 105420 (2023).
37. Cai, X. et al. Deletion of the fih gene encoding an inhibitor of hypoxia-inducible factors increases hypoxia tolerance in zebrafish. *J. Biol. Chem.* **293**, 15370–15380 (2018).
38. Wang, Z. et al. Methyltransferase SMYD3 impairs hypoxia tolerance by augmenting hypoxia signaling independent of its enzymatic activity. *J. Biol. Chem.* **298**, 102633 (2022).
39. Li, Z. et al. Zebrafish mylipb attenuates antiviral innate immunity through two synergistic mechanisms targeting transcription factor irf3. *PLoS Pathog.* **20**, e1012227 (2024).
40. Semenza, G. L. Hypoxia-inducible factors in physiology and medicine. *Cell* **148**, 399–408 (2012).
41. Liu, X. et al. Oxygen enhances antiviral innate immunity through maintenance of EGLN1-catalyzed proline hydroxylation of IRF3. *Nat. Commun.* **15**, 3533 (2024).
42. Storz, J. F. High-altitude adaptation: mechanistic insights from integrated genomics and physiology. *Mol. Biol. Evol.* **38**, 2677–2691 (2021).
43. Semenza, G. L. The genomics and genetics of oxygen homeostasis. *Annu Rev. Genomics Hum. Genet.* **21**, 183–204 (2020).
44. Zhou, D. & Haddad, G. G. Genetic analysis of hypoxia tolerance and susceptibility in Drosophila and humans. *Annu. Rev. Genomics Hum. Genet* **14**, 25–43 (2013).
45. Simonson, T. S. et al. Genetic evidence for high-altitude adaptation in Tibet. *Science* **329**, 72–75 (2010).
46. Lawrence, E. S. et al. Functional EPAS1/HIF2A missense variant is associated with hematocrit in Andean highlanders. *Sci. Adv.* **10**, eadj5661 (2024).
47. Heinrich, E. C. et al. Genetic variants at the EGLN1 locus associated with high-altitude adaptation in Tibetans are absent or found at low frequency in highland Andeans. *Ann. Hum. Genet.* **83**, 171–176 (2019).
48. Wang, J. et al. Tet1 facilitates hypoxia tolerance by stabilizing the HIF-alpha proteins independent of its methylcytosine dioxygenase activity. *Nucleic Acids Res* **45**, 12700–12714 (2017).
49. Zhang, T. et al. Prolonged hypoxia alleviates prolyl hydroxylation-mediated suppression of RIPK1 to promote necroptosis and inflammation. *Nat. Cell Biol.* **25**, 950–962 (2023).
50. Wang, R. et al. USP38 promotes deubiquitination of K11-linked polyubiquitination of HIF1alpha at Lys769 to enhance hypoxia signaling. *J. Biol. Chem.* **300**, 105532 (2024).
51. Pauzaite, T., Wit, N., Seear, R. V. & Nathan, J. A. Deubiquitinating enzyme mutagenesis screens identify a USP43-dependent HIF-1 transcriptional response. *EMBO J* **43**, 3677–3709 (2024).
52. Liu, X. et al. OTUB1 augments hypoxia signaling via its non-canonical ubiquitination inhibition of HIF-1alpha during hypoxia adaptation. *Cell Death Dis.* **13**, 560 (2022).

53. Mennerich, D., Kubaichuk, K. & Kietzmann, T. DUBs, hypoxia, and cancer. *Trends Cancer* **5**, 632–653 (2019).
54. Xie, H. et al. USP13 promotes deubiquitination of ZHX2 and tumorigenesis in kidney cancer. *Proc. Natl. Acad. Sci. USA* **119**, e2119854119 (2022).
55. Jiang, W. et al. UBL7 enhances antiviral innate immunity by promoting Lys27-linked polyubiquitination of MAVS. *Cell Rep.* **42**, 112272 (2023).
56. Kong, L. et al. The ubiquitin E3 ligase TRIM10 promotes STING aggregation and activation in the Golgi apparatus. *Cell Rep.* **42**, 112306 (2023).
57. Shearer, R. F. et al. K27-linked ubiquitylation promotes p97 substrate processing and is essential for cell proliferation. *EMBO J.* **41**, e110145 (2022).
58. van Loon, N. M., Lindholm, D. & Zelcer, N. The E3 ubiquitin ligase inducible degrader of the LDL receptor/myosin light chain interacting protein in health and disease. *Curr. Opin. Lipidol.* **30**, 192–197 (2019).
59. Bretscher, A., Edwards, K. & Fehon, R. G. ERM proteins and merlin: integrators at the cell cortex. *Nat. Rev. Mol. Cell Biol.* **3**, 586–599 (2002).
60. Luo, W. B. & Semenza, G. L. Pyruvate kinase M2 regulates glucose metabolism by functioning as a coactivator for hypoxia-inducible factor 1 in cancer cells. *Oncotarget* **2**, 551–556 (2011).
61. Zhang, J. et al. VHL substrate transcription factor ZHX2 as an oncogenic driver in clear cell renal cell carcinoma. *Science* **361**, 290–295 (2018).

Acknowledgements

We thank Cyagen Biosciences Inc. (Guangzhou, China) for assistance with the generation of *Mylip*-deficient mice. We are grateful to Drs. Peter J. Ratcliffe, William Kaelin, Amato Giaccia, Eric Huang, and Navdeep Chandel for the generous gifts of reagents. We thank Fang Zhou at the Core Facility of the Institute of Hydrobiology for the confocal microscope. This work was supported by grants from the National Natural Science Foundation of China (32473147 and 32430108), and the Major Project of Hubei Hongshan Laboratory (2022hszd001).

Author contributions

W.X. and J.W. conceived and designed the study, analyzed data, and wrote the manuscript. J.L. contributed to most aspects of the experiments. Z.L., X.L., Z.L., Y.S., L.Y., Y.W., R.Y., and F.L. contributed to various aspects of experiments.

Competing interests

The authors declare no competing interests.

Additional information

Supplementary information The online version contains supplementary material available at https://doi.org/10.1038/s42003-025-08200-x.

Correspondence and requests for materials should be addressed to Jing Wang or Wuhan Xiao.

Peer review information *Communications Biology* thanks Joachim Fandrey, Jeong-Hoon Kim, and the other, anonymous, reviewer for their contribution to the peer review of this work. Primary Handling Editor: Johannes Stortz. A peer review file is available.